

Characterization of Hidden Paint Layer Topography Using a Stereographic XRF Approach

Jennie R. Allred

Technische Universiteit Delft

CHARACTERIZATION OF HIDDEN PAINT LAYER TOPOGRAPHY USING A STEREOGRAPHIC XRF APPROACH

by

Jennie R. Allred

in partial fulfillment of the requirements for the degree of

Master of Science
in Materials Science and Engineering

at the Delft University of Technology,
to be defended publicly on Thursday December 21, 2017 at 12:00 PM.

Student number: 4518780
Supervisor: Prof. dr. J. Dik
Thesis committee: Prof. dr. J. Dik, TU Delft
Prof. dr. M. Janssens, TU Delft
Joost van Dam MSc, TU Delft

This thesis is confidential and cannot be made public until December 20, 2017.

An electronic version of this thesis is available at <http://repository.tudelft.nl/>.

ABSTRACT

Scientific investigation of paintings has been facilitated by the development of advanced non-destructive imaging methods. Characterization of painting stratigraphy traditionally requires extraction of small paint samples, thereby limiting its use to a few locations on a painting due to its destructive nature. Alternatively, non-destructive analysis of paint layer stratigraphy and structure across an entire painting often requires highly specialized and costly equipment, and/or the transport of priceless artworks. In addition, most methods are also typically limited to a localized point analysis.

This document proposes an alternative method for the substructure examination of paintings using a mobile macro-XRF spectrometer and a stereographic approach with reduced step sizes. This is coupled with a novel data analysis method which will enable a global study of the topographical features of hidden paint layers. As a prototype to test the feasibility of the method, we utilized a two-layer test sample consisting of pastose bone black pigment on pastose lead white, with an aluminum substrate. High resolution 3D optical microscopy was utilized to establish a ground truth for the thicknesses of both paint layers.

Through successful registration of MA-XRF scans obtained with varying detector geometries into a single hybrid image, we were able to find a strong correlation between the quantitative height data obtained with optical microscopy and our hybrid XRF image. Our findings indicate that utilizing this approach for visualizing hidden paint layer topographies proves to be very promising. Coupled with novel data fusion algorithms and visualization techniques, additional insight about painterly technique can thus be gained by utilizing existing MA-XRF scanners to scan a painting in multiple orientations.

PREFACE

I moved to the Netherlands in July of 2015 and soon thereafter began with the Master program in Materials Science and Engineering with a focus in sustainable energy technologies. As I drew closer to the end of my coursework, I began searching for projects to take part in for my thesis work. I have always taken an interest in the field of art, so when I was presented with an opportunity to work with Prof. dr. Joris Dik on a novel topic that would be relevant for the investigation into historic paintings, I was thrilled. While working on this project, I was able to assist with research into Frans Hals paintings using MA-XRF in the Frans Hals museum in Haarlem. This experience was invaluable, as it helped me to gain a thorough understanding of the equipment and technology used for this project.

There are several people without whom this thesis would not have been possible. I would like to thank Joris for the opportunity to work with him on this project. He was immensely helpful and ensured that I always had the resources I needed at my disposal. Prof. dr. R.G. Erdmann worked tirelessly to develop the data processing methods that were utilized for this project; the results that were achieved would not have been possible without him. His personal and academic support will forever be appreciated.

Last but certainly not least, I would like to thank my parents and my stepfather for ensuring I was able to realize the completion of my Master's degree. I could not have done it without any one of them.

*Jennie R. Allred
Delft, December 21st 2017*

CONTENTS

1	Introduction	1
1.1	Research Background	1
1.2	Areas of Importance	2
1.3	Objectives and Research Goals	2
1.4	Research Limitations.	2
1.5	Report Structure	3
2	What Is a Painting?	5
2.1	The Structure of Paintings	5
2.2	Examination of Paintings	7
2.2.1	Scientific Analysis	7
2.3	For Authentication	8
2.4	Conservation and Restoration.	9
2.4.1	Moisture.	9
2.4.2	Metal Soaps	9
3	X-Ray Fluorescence Spectroscopy	11
3.1	Production of Characteristic Fluorescent Radiation.	11
3.2	X-ray Absorption and Depth Analysis.	13
3.3	The XRF Spectrometer	14
3.4	XRF Analysis	15
3.4.1	Qualitative Analysis.	15
3.4.2	Quantitative Analysis.	16
3.5	Elemental Distribution Maps	16
3.5.1	Counting Statistics and Detection Limits	16
4	State of Research	19
4.1	Two-dimensional Analysis of Subsurface Paint Layers	19
4.1.1	Macro X-ray Fluorescence Spectroscopy	19
4.1.2	X-ray Radiography and Infrared Reflectography	21
4.2	Techniques for Study of 3D Subsurface Structure	21
4.2.1	Confocal XRF	21
4.2.2	THz Time Domain Spectroscopic Imaging	22
4.2.3	Synchrotron Computed Tomography and Computed Laminography	23
4.2.4	Pump Probe Microscopy.	24
5	Image Registration	27
5.1	Characterization	27
5.2	Automatic versus Interactive Methods	27
5.3	Homography in Computer Vision.	28
5.4	Random Sample Consensus.	29

6	Experimentation Methodology	31
6.1	Sample Preparation	31
6.2	Mount Design	31
6.3	Surface Characterization.	32
6.4	Acquisition of Elemental Maps	33
7	Sample Geometry Considerations	37
7.1	Determination of Hidden Paint Layer Elemental Composition.	37
7.2	Changes in Perspective of Sample Features	37
7.3	Target Geometry	38
8	Data Processing and Image Registration	41
8.1	Overview	41
8.2	Additional sample preparation	41
8.3	Inkscape registration.	42
8.3.1	Automated registration of elemental XRF maps	42
8.4	Optimization through correlation analysis.	42
8.5	Producing hybrid elemental intensity image.	44
8.6	Registration of XRF Image to Height Map	45
9	Results	47
9.1	Preliminary XRF scans	47
9.2	Registration of XRF maps to Height Maps	47
10	Discussion	51
10.1	Reproducibility	51
10.2	Feature detection in XRF images and surface painting	52
10.3	Experimental Error	52
10.4	Recommendations	52
10.5	Conclusions.	53
	Bibliography	55

1

INTRODUCTION

1.1. RESEARCH BACKGROUND

Paintings are widely considered to be one of the most important elements of cultural heritage and as such there has been an increasing level of study into their make-up over the past century, with rising intensity occurring over the span of the past few decades. More recently, the investigation of ancient and modern artworks using non-invasive analytical techniques has become a widely researched topic for the fields of art history and conservation science. Knowledge of the materials used can assist conservators with ensuring that the works are appropriately cared for during ongoing housing and conservation efforts and provide the ability to ascertain authenticity. Information about the layer structure and the materials used in the creation of art not only provides insights that are useful in their conservation, it can also present a way to envision the creative process of the artist. In particular for paintings, clues as to how the methods used by painters changed over time as well as insights into the evolution of their style of painting can be determined.

Many artists are also known to have frequently reused painting supports by painting over an existing composition. It is estimated that around twenty percent of old master paintings have an earlier work by the artist painted underneath. These hidden paintings are difficult to characterize in terms of paint layer stratigraphy and surface topography; it is not possible to scrape away the top layer to investigate the underlying painting. This information is relevant for obtaining a complete picture of the work under investigation, however. An artists modus operandi is ascertained through the study of his working process, which cannot be fully understood through visual observation of a finished painting. Therefore, a virtual reconstruction of the underlying painting is necessary. A thorough technical characterization can assist in an improved assessment of the painters working methodology, or even help with the authentication of attributed or suspected works. Knowledge of the materials and processes used to create a painting help to ensure that the correct treatment and housing methods are utilized in its care. Before a painting can undergo any restoration or cleaning processes, it is important to have a full understanding of any damage or defects, previous treatments, and materials used through an examination of the paintings current state. A proper understanding of the full extent of materials and processes used helps in guiding the efforts of the conservator, ascertaining authenticity or attribution, and in establishing more knowledge about the artist himself. A cooperation between scientists, conservationists, and art historians has played a crucial role not only in ensuring that appropriate care and restoration techniques are administered to pieces of cultural heritage, but also for assisting in ascertaining knowledge of the working methods and techniques used by the artist.

Macro-XRF (MA-XRF) is a method of investigation that has become a prominent choice in many museums for ascertaining the elemental composition of pigments in paintings. The advent of mobile MA-XRF devices enables *in-situ* examination and is preferential to the transport of historical artworks. Until now, the benefits of MA-XRF have been limited to a 2D analysis of pigments.

In this research, an assessment of the current state of technology for the thorough characterization of the materials present in a painting as well as the ability to visualize the 3D subsurface topography and structure of hidden paint layers will be conducted, followed by a proposal for a new method of investigation using MA-XRF that will enable both of these critical factors to be examined in repeatable studies.

1.2. AREAS OF IMPORTANCE

The impact of this research is not limited to the study of paintings. Numerous fields have a need for the ability to acquire the elemental and structural composition of materials. The automotive and aerospace industry use complex laminate materials which necessitates the detailed investigation of structural, surface, and interfacial properties. Concrete is one of the most widely used construction materials and has a complex pore structure, the investigation of which is important for ascertaining durability related to mechanical and fracture toughness properties [1]. Planetary scientists use 3D imaging techniques to investigate meteorites, mission returned samples, and other planetary materials [2]. The medical community has utilized 3D imaging technology since the early 1970s and continues to be a leading field for its implementation [3].

1.3. OBJECTIVES AND RESEARCH GOALS

An assessment of the literature on methods available for the analysis of hidden paint layers will be conducted in order to gain a better understanding of the current state of research.

Primary Objectives Investigate a painting using the non-destructive and well-established scientific technique of MA-XRF with the goal of creating digital 3D visualizations of the topography of hidden paint layers.

Secondary Objectives In order to realize the goals of this thesis and provide a clear account of the research, the primary objective will be divided into four secondary objectives as follows:

- Use a quantitative method on a visible paint layer to establish a ground truth thickness that can be used as a reference for comparison to MA-XRF scans.
- Simulate a multiple detector MA-XRF setup
- Create a 3D visualization of a hidden paint layer
- Relate the MA-XRF scans to quantifiable data in order to establish validity of research

1.4. RESEARCH LIMITATIONS

This thesis research must be conducted within an eight month time-frame, and access to the MA-XRF scanner that will be used for experimentation is limited. Therefore, experiments must be well-planned and coordinated with additional unrelated research it is being utilized for.

1.5. REPORT STRUCTURE

After this introductory chapter, the report follows with background information on the development of paintings, including the methods and materials used for construction in chapter 2. This chapter will also detail common scientific methods employed for achieving a deeper understanding of paintings as well for authentication purposes, and lastly some of the more common degradation mechanisms that painting conservationists face.

Chapter 3 provides background information on the theory and techniques used for XRF analysis

Chapter 4 contains a literature review with a survey of the methods that have been used for the sub-surface analysis of paintings.

Chapter 5 introduces the reader to image registration, one of the key components of this research. An overview of the mathematical concepts and the data processing techniques used for automated image registration will be discussed.

Chapter 6 describes the test sample preparation, experimental setup, equipment specifications, and parameters used for the MA-XRF scans.

Chapter 7 addresses the sample and setup geometry and the effect it has on the registration processes used in this research.

Chapter 8 presents the data processing methods that were employed to realize the ultimate goal of this research: Creating digital 3D visualizations of the topography of hidden paint layers.

Chapter 9 presents the research findings and results of the data processing, with visualizations of the virtual reconstructions.

Finally, the thesis is summarized in chapter 10, where the significance of the thesis, recommendations for future works, and recommended improvements to the existing methodology can be found.

2

WHAT IS A PAINTING?

Paintings are constructed using a variety of materials that are typically influenced by the time period in which the painting was composed. The architecture of a painting has a measured effect on the applicability of suitable techniques for scientific analysis, and as such the breadth of artistic materials used must be considered. Section 2.1 discusses the methods and materials used for the construction of paintings, section 2.2 provides a brief introduction to the scientific analysis of paintings, section 2.3 discusses the relevance of scientific investigation for authentication purposes, and 2.4 explains some of the degradation mechanisms that painting conservationists face.

2.1. THE STRUCTURE OF PAINTINGS

Paintings are usually 2D representations of an object, narrative, or idea, and are typically constructed on a flat rectangular surface. As seen in figure 2.1 a painting typically consists of a support with a layered build-up of size, ground layer, a preliminary sketch, paint layers, glaze, and then varnish.

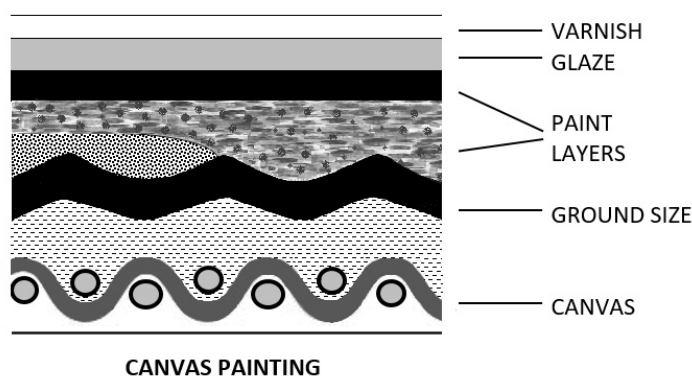


Figure 2.1: A cross section showing the structure of an easel painting

The support is the material chosen to construct the painting on. A commonly used support material is linen canvas, which is typically stretched onto a wooden frame before or after completion of

the painting. Rigid supports are also used and can include wooden panels, metal, glass, plastic, or other materials. The type of support used will have a measured effect on the techniques that may be utilized to examine the painting; rigid supports made of a material such as wood or metal will not allow for the same methods of investigation that linen canvas will, namely those involving transmission techniques. Easel paintings are those which could be created by placing the support on an easel, as opposed to a wall fresco or a large panel painting, such as those found in cathedrals, which were commonly stationed on the floor during the painting process. For reasons of practicality, the scope of this research will focus on easel paintings which do not have any limitations in terms of movement.

The support is prepared for the application of paints by applying *size*, which is a diluted glue typically made from animal skins and which is designed to protect the support from absorption of the ground. Size provides a barrier for absorption of the ground layer by the support, and is most commonly a water-based glue derived from animal skins. In addition, size protects the support material from being weakened by the build-up of the subsequent layers of the painting. For paintings on canvas, the application of size also assists in shrinking the canvas into a smooth, taut surface once it dries.

The ground layer provides further protection for the support from the organic paint layers and is usually gesso—a mixture of glue, calcium carbonate, and often a white pigment; white lead was used until its replacement by the less toxic titanium white in the twentieth century. Another benefit of this layer is to provide a smooth surface for the artist to paint on; linen canvas in particular has a woven structure that is more apparent without the use of a ground layer.

Artists often sketch their vision for the painting onto the ground layer using lead, charcoal, metal point, or dark paint. This underdrawing serves as a guide for the application of paint layers that will form the final composition. Following the ground layer and any underdrawing is the application of paints—ground up pigments contained in a transparent binding medium. Binder materials vary but typically consist of oils, waxes, egg, resins, plant gums, or other materials. The paint layers are added successively over one another to create different visual effects as desired by the artist.

Until the mid-19th century, the range of pigments used by artists was not expansive; the typical palette usually consisted of around ten different paints. The pigments used can be divided into four basic categories: earths, minerals, manufactured, and organic. Earth pigments typically consisted of iron, manganese dioxide, alumina, and silica. These were used in abundance on many paintings and were relatively inexpensive to obtain. Minerals provided the rich and brightly colored pigments for many of the blues, yellows, and reds. Orpiment provided an iridescent yellow, blues commonly consisted of ultramarine or azurite, the former of which was made by grinding the mineral lapis lazuli, and cinnabar was used for the red pigment vermilion. Manufactured pigments include the whites used for the ground layer and most white paints, which were comprised of lead carbonate (PbCO_3).

Organic pigments include the range of blacks made from charcoal or charred animal bones or by burning oils or resins; the lake pigments were made from ground up dried insects. After the surge in scientific advances in the 19th century, artists were able to access to a much wider range of pigments. Many that had been used for centuries were replaced with less toxic, cheaper alternatives.

Paint layers can range from tens of microns to millimeters thickness. Impasto is a technique used by painters in which thick, broad strokes are applied with a paintbrush or palette knife to achieve texture that is immediately evident when viewing the work. This build-up of paint creates a 3-dimensional effect that is unique to paintings constructed in this manner. Paintings by the Dutch

artist Vincent van Gogh, for example, commonly contain highly textured surfaces resulting from the application of thick paint layers. His painting *Wheat Field with Cypresses* is an excellent example of the deployment of this technique and is shown in 2.2. These surface relief features have a measured effect on how the pigments contained in the paints are perceived and as such are an important aspect of the painting.



Figure 2.2: Vincent van Gogh's *Wheat Field with Cypresses*

Application of a glaze over the paint layers is optional but can improve the appearance of the painting by refracting light from the underlying paint layers which has the effect of creating deep, rich colours. Varnish helps to reduce the impacts of moisture, dirt, atmospheric pollutants, and surface abrasions and is applied as a protectant for the painting.

2.2. EXAMINATION OF PAINTINGS

When we observe a painting with the naked eye, we are only able to see what the artist intended for us to see. The final composition does not always strictly adhere to the underdrawing, which can be an indication of a change from the artists original intent. In addition, painters frequently reuse the supports of finished works by painting a completely new composition over an existing one, whether for economic reasons or simply because they were not satisfied with one of their creations. These hidden paintings have immense historical value, and are the subject of much research by art historians and scientists alike.

2.2.1. SCIENTIFIC ANALYSIS

In the late 19th century researchers first became interested in performing scientific analysis on paintings in an effort to better understand them. X-ray radiography (XRR) was and still remains a popular and straightforward investigation method for paintings. The first recorded case of XRR being used on a piece of cultural heritage was in 1896 by physicist Walter Koenig to examine the

structure of a collection of artifacts in the Senckenberg Museum of Natural History in Frankfurt Germany [4]. Many years later, Pablo Picasso's painting *The Old Guitarist* was examined with XRR and proved to have an underlying sketch of a mother and child underneath the visible painting. Following this discovery the use of XRR was identified as a practical means for examining the under drawings or compositions hidden beneath visible paint layers in paintings.

Infrared Reflectography (IRR) was developed in the late 1960s by the Dutch physicist J.R.J. van Asperen de Boer, to improve upon the results of infrared photography [5]. It is a non-invasive and non-destructive technique that enables the visualization of any underdrawings or pentimenti within the painting. This not only assists in the quest for information about the working process of the artist as they build up a composition, it has also led to the discovery of unknown or assumed lost works from their repertoire. A large number of paintings have been proven to contain entirely different compositions underneath the one visible to the naked eye, which has resulted in an increase of research specifically aimed at learning more about these hidden works. Chapter 4 will discuss some of the research that has been performed in further detail.

2.3. FOR AUTHENTICATION

In 1930 L. van Puyvelde of the Royal Museum of Fine Art of Belgium in Brussels used XRR on an acquired Daniel Seghers painting entitled *Guirlande de Fleurs*, which portrayed the figure of a woman surrounded by a garland of flowers. The woman was painted in such a way that suspicion was aroused as to whether she was part of the original painting, or rather an addition by a later artist. Upon radiographic investigation, it was indeed ascertained that a depiction of a nativity scene was covered by the over-painting of the woman. This new information, coupled with the expertise of the art historians that first questioned the authenticity of the painting, led to the eventual removal of the subsequent paint layer which restored the piece to its original integrity [6]. This was one of the first recorded cases of X-rays being utilized to determine the authenticity of a painting.

Later in the twentieth century, more advanced and diverse methods for the scientific study of cultural heritage began to see widespread use in museums and research facilities. Raman spectroscopy was first used to determine the elemental composition of a piece of cultural heritage in 1979 when P. Dhamelincourt et. al. examined an ancient Chinese vase, however the technique would not be prevalently used by art researchers until Ian M. Bell et. al published a comprehensive paper detailing the characterization of 56 pigments frequently used in paints [7] [8] [9].

More recently, a team of researchers from the Netherlands and Belgium performed MA-XRF on a disputed Van Gogh in 2008 in order to analyze a hidden painting of two wrestlers that was previously identified using X-Ray radiography. Using new information obtained from these scans paired with diary entries and letters to his brother, historians were able to definitively attribute the painting, *Still Life with Meadow Flowers and Roses*, to Van Gogh [10]. In addition, works of questionable provenance can be examined more thoroughly with scientific equipment and techniques than with the naked eye. Anachronistic materials can be easily identified with certain techniques, making it virtually impossible to stage a forgery of an historic painting without access to the pigments used during that time period. Most historic and modern pigments have been studied and there is consequently a wealth of information about the periods in which they were used, the methods and materials used for preparation, and precisely when they were used. An accurate identification of the materials in a painting provides the ability to compare chemical data to historical data, increasing confidence in an authentication analysis. Scientific examination plays an important role in the process, but it cannot tell the whole story. The knowledge of art historians is a key component for a

true understanding of the bigger picture.

2.4. CONSERVATION AND RESTORATION

Knowledge about the stratigraphy of a painting is vitally important for the application of appropriate conservation techniques. Naturally occurring mechanisms can have a negative impact on the stability of a painting and early detection of any issues provides information that may assist in repair or prevention of further deterioration. Damage can be incurred in numerous ways, ranging from physical impact to environmental degradation. Air pollutants, the radiant energy from light, moisture, temperature, and other characteristics of the surroundings all have an effect on the materials used in a painting's construction. Surface damage is relatively simple to characterize with currently existing methods, however subsurface damage is more difficult to distinguish and less research exists in this area. This section will discuss areas of concern for subsurface damage to paintings which could benefit from further research into solutions for detection.

2.4.1. MOISTURE

Canvas paintings have been shown to be particularly susceptible to moisture uptake causing them to exhibit significant dimensional changes and internal stresses; at high humidity the canvas may shrink while the other layers of the painting may have a tendency to swell, leading to cupping. Studies have been conducted into the effect of temperature and relative humidity on the internal stress variations in paint layers [11] in an attempt to learn how to lessen the consequences from it.

2.4.2. METAL SOAPS

The degradation process in paintings involving the formation of metal soaps is a long-standing issue in the conservation of oil paintings. The Tate Museum in London estimates that over 60 percent of its collection of early 16th century-17th century paintings suffer from damage incurred by lead soap inclusions. Lead, copper, zinc, aluminum, iron, alkaline, and alkaline earth metals found in pigments react with the fatty acids contained in the binding medium to form carboxylates. These metal carboxylates exist as small inclusions in the paint layers that can migrate over time, eventually rising to the surface of the painting and causing degradation to its appearance. They can also cause delamination of paint layers [12].

Heat, light, and humidity all accelerate the formation of these compounds by causing the negatively charged fatty acids to separate from their glycerol backbone and diffuse through the paint layers, where they eventually combine with the positively charged metal cations. If the metal ions merge with the fatty acids at the surface of a painting, it can cause a black crust to form that cannot be removed with traditional cleaning solvents [13]. Metal soaps are not only a concern for old master paintings as they can be found in modern day oil paintings as well. Early detection of these damaging compounds and their location within paintings could assist in the prevention of damage, and is the subject of ongoing multidisciplinary research [14]. Figure 2.3 shows evidence of metal soap formation and the damage incurred by it across Rembrandt's *Anatomy Lesson of Dr. Nicolaes Tulp*.



Figure 2.3: Rembrandt's *Anatomy Lesson of Dr. Nicolaes Tulp*, with examples of the damage caused by the formation of metal soaps within the painting.

3

X-RAY FLUORESCENCE SPECTROSCOPY

X-ray Fluorescence spectroscopy is one method commonly employed to conduct an element-selective 2D analysis of artifacts, which enables scientists to create digital reconstructions based upon historical pigment databases. This chapter provides background information on the working principles, equipment, and data analysis procedures for XRF spectroscopy, which is the technique that will be utilized for the imaging of the interfacial topography of hidden paint layers in this research.

3.1. PRODUCTION OF CHARACTERISTIC FLUORESCENT RADIATION

XRF spectroscopy is a non-destructive analytic technique used to evaluate the elemental composition of a wide array of materials by irradiating a sample with X-rays while simultaneously capturing the emitted radiation. Typically, the source is an X-ray tube but synchrotron sources are also used for high resolution scans with short per-pixel dwell times, enabling megapixels per hour scans.

As the elements in a sample are bombarded with X-ray energies above the element's binding energy, they will emit characteristic fluorescent X-rays (see figure 3.1). This emitted radiation has a discrete energy that is recorded and subsequently used to identify the elements present in a sample.

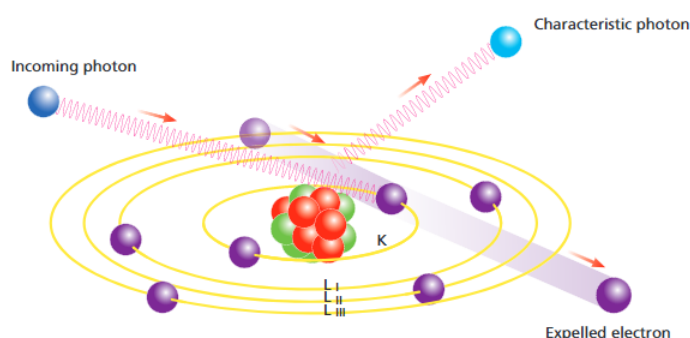


Figure 3.1: Production of characteristic radiation

The energy of any electron in an atom depends upon the shell it normally occupies within the atom. Incoming X-ray photons or electrons with high enough energy can cause an electron to be expelled from the atom, which produces a hole in one of the atom's shells. This vacancy results in an unstable energy configuration, which is made stable again when a higher energy electron transfers to the lower energy shell. A $K_{\alpha 1}$ X-ray, for example, arises when there is a vacancy in the

K-shell and an electron drops from the M_3 shell to fill it. The atom then emits an X-ray with energy: $E_{X\text{-ray}} = E_K - E_{M_3}$. Figure 3.2 shows a simplified diagram of the electron transitions which can occur when irradiating a sample using XRF techniques.

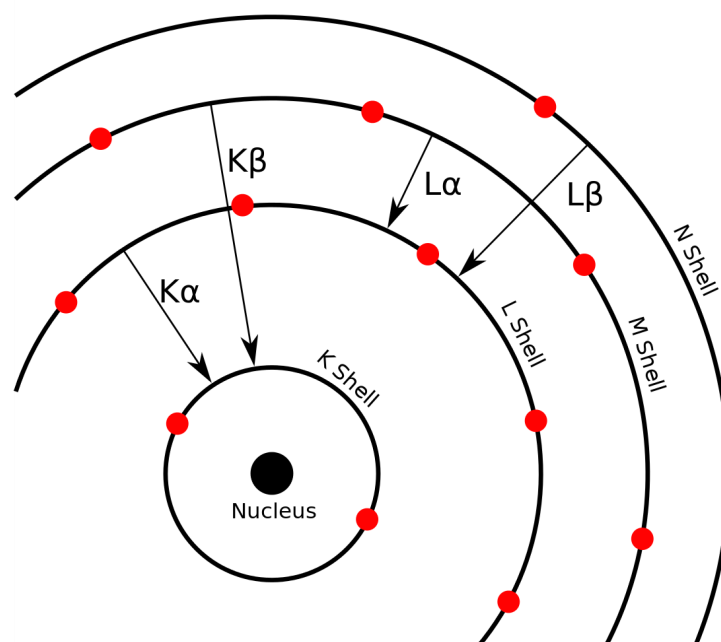


Figure 3.2: Schematic of Electron Transitions

There are specific ways that these electron transitions may occur, for example a transition from the L1 to the K shell is not possible due to quantum mechanical considerations. In addition, it is not always the case that a vacancy created by the incoming X-rays will produce fluorescent photons. There are several ways to notate the different transition lines, however the Siegbahn notation is most commonly used in literature. It uses a Greek letter to indicate the intensity of the line, which is added as a subscript to the letter referencing the shell with the chemical symbol of the element indicated as well. For example, Pb K_α is the most intense line due to an expelled K electron. Figure 3.3 provides a graphical overview of the most important electron transition lines in Siegbahn notation.

The fluorescent yield is a function of the atomic number (Z) of an element and increases correspondingly. The highest yield occurs when the incoming photon energy is just above the energy of the electron expelled from the atom. Most elements are detectable using XRF spectroscopy, however light elements with Z less than 12 produce very low yields and as a result are difficult to detect. Therefore, detection of pigments containing organic compounds must be performed using other techniques. Surface-enhanced Raman Spectroscopy (SERS) has been increasingly used as a method for identification of lower Z elements [15] with favorable results.

The vacancies that are initially created by incoming radiation do not always produce fluorescent photons, even if the energy of the incoming photon is high enough to expel electrons from the atom. The *Auger* effect occurs when an electron from a higher energy level falls into the vacancy created by incoming radiation, but instead of releasing energy as a photon, the energy is transferred to another electron which is subsequently ejected from the atom. *Compton scatter* is the inelastic scattering of a photon and results in a decrease of energy.

The fluorescent yield depends on the thickness, density, and composition of the material under investigation and can be calculated as the ratio of the number of fluorescent photons ejected from

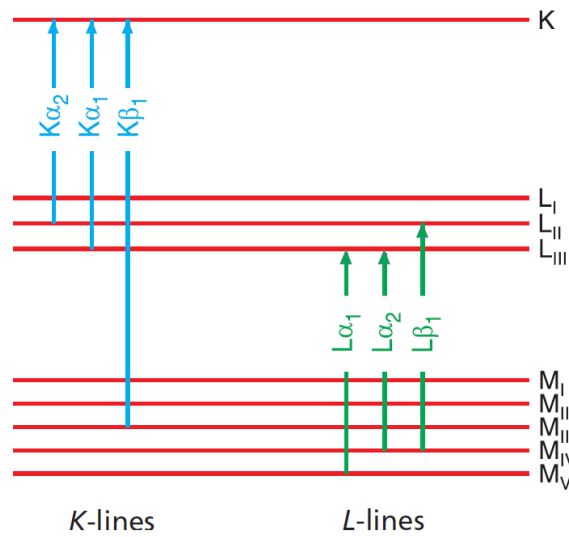


Figure 3.3: The major electron transitions and their corresponding K-,L- lines

the atom to the number of initial vacancies. This is shown graphically in figure 3.4 for the K- and L- lines.

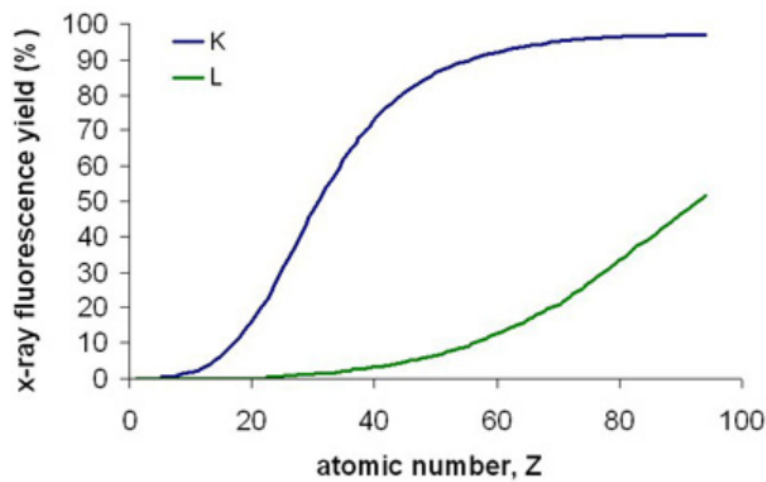


Figure 3.4: Illustration of the K and L fluorescence yield as a function of atomic number, Z. It is clear that the yield for the light elements is very low, which is reflected in the achievable sensitivity for these elements.

3.2. X-RAY ABSORPTION AND DEPTH ANALYSIS

In order to characterize subsurface paint layers, X-rays must be able to penetrate any outer paint layers and subsequently any radiation produced must be able to escape back out and reach the detector. Some radiation will be absorbed by the outer paint layers during both of these processes. X-rays are absorbed as they pass through matter in accordance with exponential law:

X-rays are absorbed as they pass through materials according to the exponential law:

$$I = I_0 e^{-\mu x} \tag{3.1}$$

where I_0 is the incident intensity, I is the reduced intensity after travelling a distance x through a

material, and μ is the absorption coefficient. For any given element μ increases with atomic number Z and X-ray wavelength. This absorption effect is commonly referred to in XRF elemental maps as shielding.

3.3. THE XRF SPECTROMETER

The fundamental components of an XRF detection system are a source, sample, and detection system. The X-ray source irradiates a sample with high energy X-rays from a controlled X-ray tube, and the detector measures the radiation emitted from the sample. A simplified schematic of the setup for XRF can be seen in figure 3.5. In the majority of cases the source consists of an X-ray tube, however for more precise and higher energy X-rays a synchrotron source is sometimes utilized. Due to the difficulty of transporting works of art, the use of synchrotron facilities is generally limited to examination of small painting samples that have been removed or recovered from paintings [16].



Figure 3.5: Schematic of a typical XRF setup

The detector directly measures the electron counts of the incoming radiation. The three most important properties of the detector in an XRF spectrometer are the *resolution*, *sensitivity*, and *dispersion*.

The *resolution* of a detector refers to its ability to make a distinction between the different energy levels of fluorescent photons. A detector with a high resolution signifies that it has the capacity to distinguish a wide range of energy levels.

Sensitivity is an indication of how efficiently incoming photons are counted. If a detector is not sufficiently thick, incoming photons might pass through it without detection. The fluorescent X-rays emitted from the sample are captured by the detector, which emits a distribution of pulses whose voltages are proportional to the incoming photon energies. Sensitivity can be quantized as the ratio of the number of pulses to the number of incoming photons.

Dispersion is the separation of the different energies of the incoming photons. A high dispersion indicates that different energies are separated well.

In addition to fluorescence, scattered tube radiation also reaches the detector, which results in background noise. This background noise often results in low intensity peaks coinciding with elements present in low concentrations, making it more difficult to establish their existence within the sample. A set of software programs and Python modules belonging to *PyMca* was developed specifically to circumvent this common issue with fluorescent intensity readings and is a well-established tool for interpreting XRF data. With *PyMca*, Coster-Kronig and Auger transitions are correctly accounted for as well, increasing the accuracy of the fluorescent counts.

An example of an XRF spectrum that was obtained using a hand-held spectrometer during the in-

investigation of a Bernardo Martorell painting is shown in figure 3.6. Every transition of an electron to a lower energy shell within an atom carries with it a specific voltage, which can be observed in these energy spectrums as a peak. The elements that are contained within a sample can be ascertained by examining the peaks that are present within the spectrum.

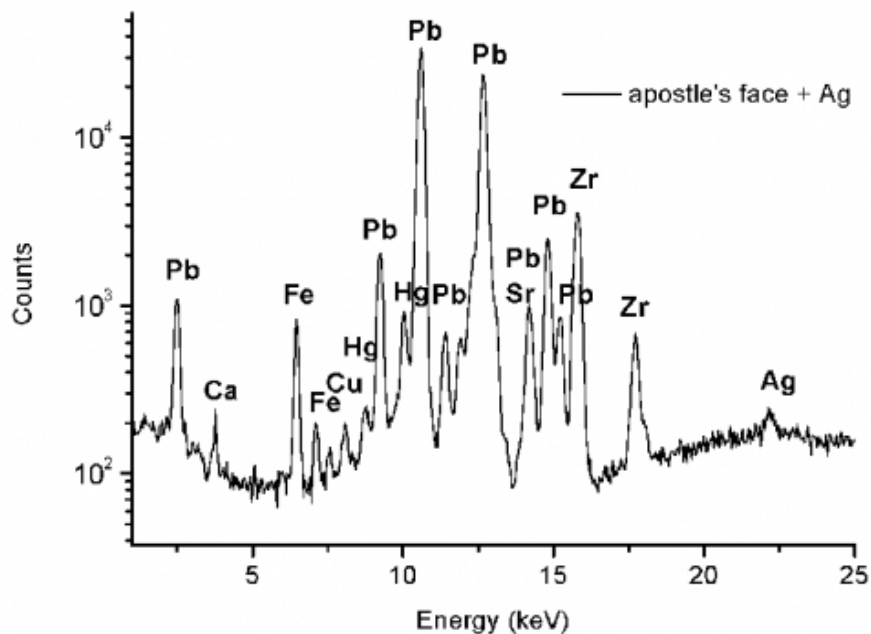


Figure 3.6: XRF Spectrum for a Bernardo Martorell painting showing peaks for the elements present in the painting

3.4. XRF ANALYSIS

Once a sample has been scanned with XRF, the data is then analyzed. This takes place in two stages: First with qualitative analysis and then with quantitative analysis. Qualitative analysis determines which elements are present within the sample as well as their net intensities from the measured spectra. The net intensities are used in the quantitative analysis to calculate the concentrations of the elements present. The following sections will provide a brief overview of the methods employed to perform these analyses.

3.4.1. QUALITATIVE ANALYSIS

Qualitative analysis is used for determining which elements are present in a sample that has been scanned using XRF. The following subsections will describe the processes involved for resolving the peaks in an XRF spectrum.

PEAK SEARCHING AND PEAK MATCHING

Peak searching utilizes a mathematical technique to find which peaks are present in any given spectrum. Peak matching determines which elements belong to the peak profiles obtained from an XRF scan. By comparing the positions of the peaks obtained to a database with information about the

positions of all possible lines for any given element, the elements present in the sample can be determined. The peaks in the spectral series are also closely observed in order to make a distinction between the different energies allowed for each element. For example, together with any K_{α} line there must also exist the K_{β} line with an energy approximately one-fifth to one-tenth the intensity.

DECONVOLUTION AND BACKGROUND FITTING

An XRF spectrometer measures the sum of the background and the profiles obtained from a scan. When two incoming fluorescent photons have a similar energy, their peaks may overlap. When this occurs, it is necessary to use a deconvolution method which resolves the spectral overlaps by determining the area of the individual profiles.

3.4.2. QUANTITATIVE ANALYSIS

To quantify the results obtained with scanning XRF, the signal processing unit takes the net intensities of the captured X-ray fluorescence and produces the spectrum. Additional software processing techniques convert the spectrum information into concentration amounts that are specific to the elements present in the sample.

3.5. ELEMENTAL DISTRIBUTION MAPS

During an XRF scan of a painting, the source beam moves along a trajectory with a designated *step size*. The step size is a key factor in determination of the pixel size of the distribution images and hence the spatial resolution. The spatial resolution can be improved if the step size is chosen to be smaller than the *spot size*, the size of the beam that strikes the sample. As the source beam moves across the painting, the concentration of the elements that were selected for analysis are computed from the net peak intensities of the electron transitions that are recorded.

To enable visualization of the concentration density of the elements which are present, the standard is to correlate high elemental concentrations with white colouring, although any colour can be chosen to represent the relative concentration of an element across a painting. As the concentration of an element decreases the colour on an XRF elemental distribution map will correspondingly transition from the selected colour to black. Figure 3.7 shows an example of elemental maps obtained from the XRF scan of a section of Caravaggio's *Supper at Emmaus*. Bright white areas indicate regions of the painting where a high concentration of a specified element is located. These images are usually simply referred to as either XRF maps or XRF images. For paintings, a direct correlation between the presence of an element and the colour that it will appear as can be made based upon knowledge obtained from a pigment database such as the one mentioned in 2.3.

3.5.1. COUNTING STATISTICS AND DETECTION LIMITS

An XRF detector counts incoming photons. The number of incoming photons is not usually uniform, so it is important to record the measurements for a sufficient period of time at each location on a painting. Measuring for a longer time period and then calculating the average per second gives a more accurate result of the concentration of elements at each location in the painting. This will lead to a more accurate representation of the elemental concentrations in the XRF images.

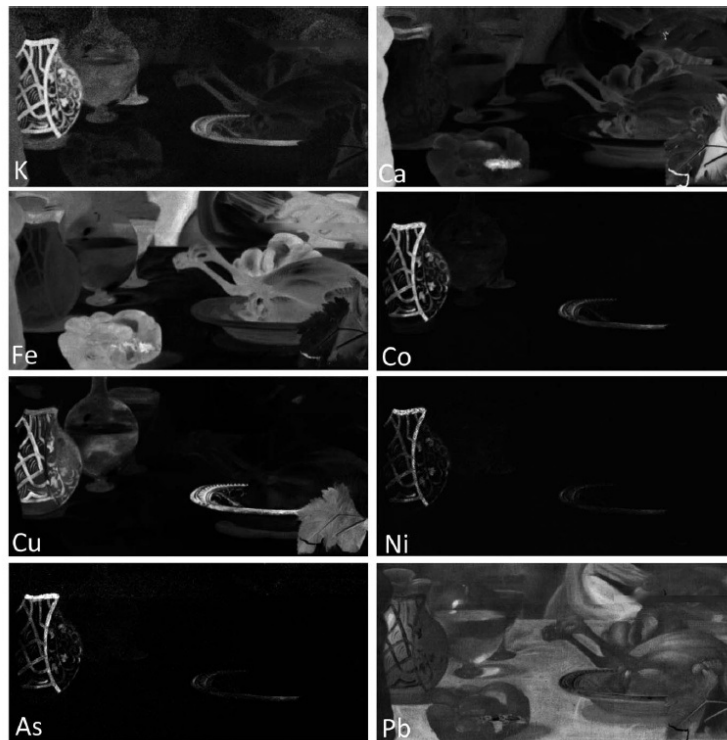


Figure 3.7: Elemental maps obtained with XRF from an area of *Supper at Emmaus* by Baroque artist M. Caravaggio. The distribution of eight elements are pictured: bright white areas coincide with high concentrations of the element indicated.

4

STATE OF RESEARCH

There are numerous techniques which have shown promising results for the depth profiling and subsurface analysis of paintings, both of which are relevant for developing a more thorough understanding of hidden compositions. This chapter discusses the current state of research into techniques that facilitate these investigations. The first section will examine the use of XRF and its current constraints, followed by a survey of other methods employed for examining hidden paintings. The remaining sections will cover an in-depth review of technologies currently employed for investigation into the 3D structure of paintings and other cultural heritage artifacts.

4.1. TWO-DIMENSIONAL ANALYSIS OF SUBSURFACE PAINT LAYERS

Numerous techniques exist for analyzing the two dimensional characteristics of what lies beneath the surface of a painting. These methods have proven to be extremely valuable for achieving a better understanding of hidden aspects of a painting. The following sections will describe the more frequently used methods in detail.

4.1.1. MACRO X-RAY FLUORESCENCE SPECTROSCOPY

Macro X-ray Fluorescence Spectroscopy (MA-XRF) has become one of the most popular methods for subsurface elemental examination of paintings in recent years [17], [18], [19]. Its first implementation on paintings was in 2004 when Z. Szokefalvi-Nagi et al. performed elemental analysis on three paintings from the Hungarian National Gallery [20]. Scanning XRF provides the ability to obtain two dimensional spatially resolved elemental distributions across an entire painting and it enables the detected pigments underneath the surface to be recorded photographically.

Synchrotron radiation based X-ray fluorescence mapping was utilized on a painting by Dik et. al in 2007 and it led to the discovery of a lost Vincent van Gogh portrait hidden underneath a painting of grass. It was revealed that underneath Van Goghs *Patch of Grass* a portrait of a woman lay hidden underneath the visible paint layers. Furthermore, observation of the elemental distribution in the hidden painting allowed for a reconstruction of the color scheme based upon knowledge of the pigments those elements were contained in with regard to Van Gogh's palette [21]. Figure 4.1 shows the results of the color reconstruction performed by the group. This ground-breaking visualization strategy paved the way for gaining additional insights from hidden paintings using XRF technology.

Thurrowgood et al. built upon this work in 2016 by creating a color image reconstruction of a newly discovered hidden Degas painting. Using custom-built software, the research group was

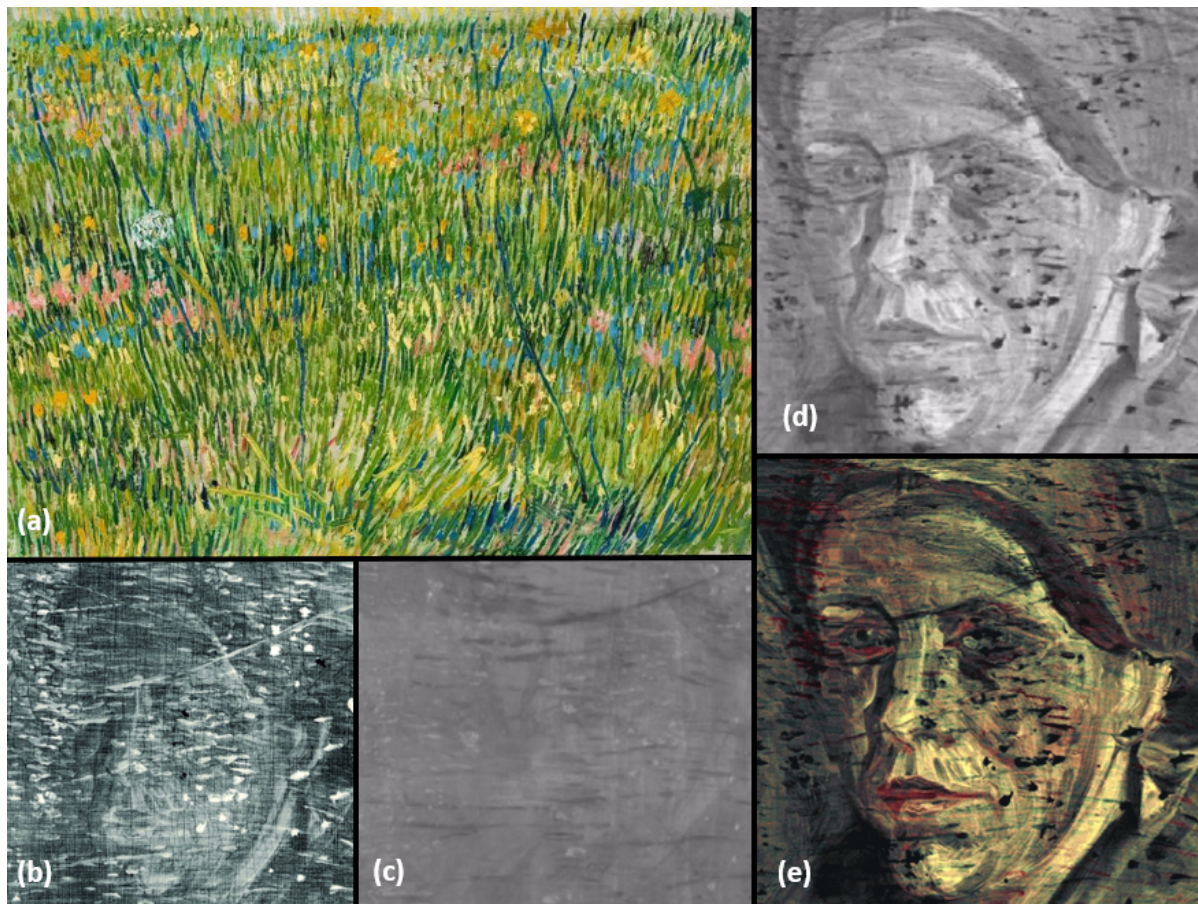


Figure 4.1: (a) Visible image of Vincent van Gogh's painting *Patch of Grass* (b) XRR obtained image of hidden figure underneath surface painting (c) IRR image of hidden figure (d) Sb- K_{α} XRF distribution map (e) Colour reconstruction of hidden figure using numerous XRF elemental distribution maps.

able to construct an image layer for each elemental map obtained using manual assignment of one pigment for each image. The results of their work are shown in figure 4.2

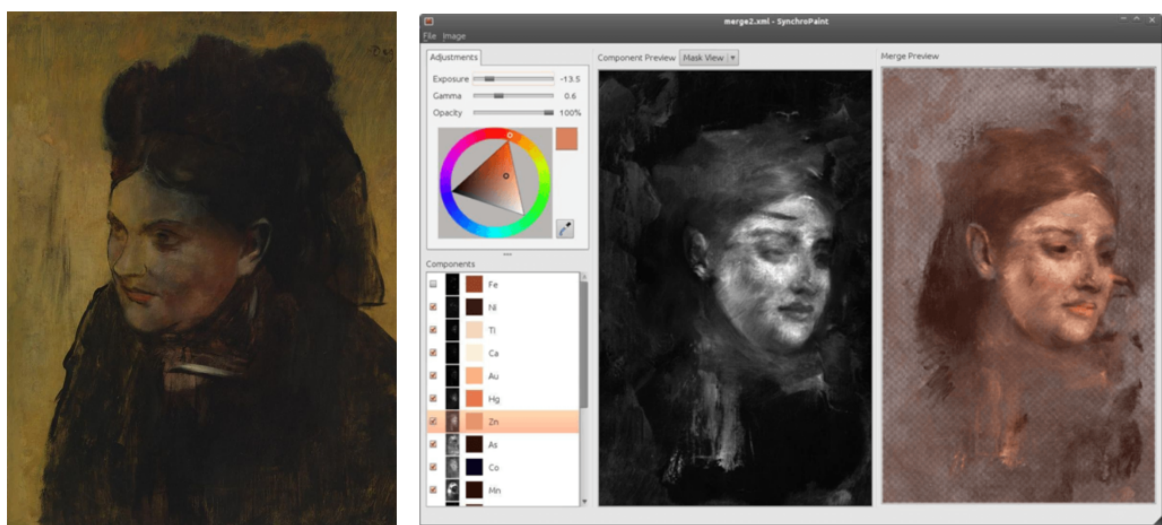


Figure 4.2

With the development of mobile units capable of scanning paintings with millisecond/pixel dwell times, museums and private collectors are able to perform in-depth studies without requiring the transport of items in their collection. As a result, more museums are purchasing or leasing equipment for the purpose of conducting research on paintings. However, in its current state mobile units have limitations in terms of subsurface analysis. So far, only two-dimensional visualizations have been executed using standard mobile XRF units.

4.1.2. X-RAY RADIOGRAPHY AND INFRARED REFLECTOGRAPHY

As discussed in section 2.2.1, XRR and IRR were the first methods used for investigating the pentimenti and underdrawings of paintings, and they are still in widespread use today in museums worldwide. However, these options are somewhat limited in their ability to study the substructure of the underpainting.

XRR works well with dense pigments such as lead white. The transmission of X-rays through a paint layer is inversely proportional to the atomic weight of the element under investigation, therefore only relatively heavy elements such as lead and mercury can stop the x-rays sufficiently enough to be visible in a radiograph. The array of pigments in historic paintings containing these elements is limited: lead white, lead-tin-yellow and vermilion (mercuric sulfide) are the most frequently used ones that are not transparent to X-rays, making this technique limited in practicality for artworks composed of a wide array of pigments. Another disadvantage of XRR is the long exposure times and the necessity of repeated trials in order to obtain a radiograph with clear details.

Infrared Reflectography is a well known and frequently used visualization technique for examining the underdrawing of paintings which relies on the fact that most pigments are transparent to infrared radiation in specific spectral ranges. However, this technique cannot provide depth information and it is sometimes hindered by thick paint layers [22]. In addition, paints containing black such as carbon black or lamp black will be opaque to IRR, limiting the inspection of paintings containing this pigment in abundance.

4.2. TECHNIQUES FOR STUDY OF 3D SUBSURFACE STRUCTURE

The most common method for examining the stratigraphy of paint layers is through the removal of a cross section of paint. This can then be examined using a variety of techniques, however it is a destructive process and can only provide information about a specific point in the painting. In order to avoid causing irreparable damage to paintings, new methods are being sought out for examining subsurface paint layers in artworks. If a technique allows for the global study of a painting it also allows for a more representative analysis. This section will review the techniques that are currently being developed for the research of the 3D structure of paintings.

4.2.1. CONFOCAL XRF

Improvements in hollow glass capillary tube-based X-ray optics [23] have enabled confocal XRF (CXRF) to emerge as a technique capable of providing information about elemental concentrations as well as depth profiles of pigment layers. Two optics are placed perpendicular to one another: one focuses the beam while the other collects fluorescence from the sample in the region where the focal cones of the two optics intersect. The sample is scanned within this moving volume to obtain composition as a function of depth. These depth-resolved measurements allow for a full 3D analysis without requiring the use of a reconstruction algorithm [24]. This can be very useful for the

examination of paintings; traditional XRF will reveal a hidden composition but no information is given concerning its location within the stratigraphy of the paint layers.

Confocal XRF was utilized at a synchrotron radiation source by Bisulca et. al [25] and it enabled the research team to perform a paint layer depth analysis on a David Teniers painting entitled *The Armorer's Shop*. To resolve the chronology of the paintings construction, multiple locations across the painting were scanned using CXRF with positive results. The results of their analysis are shown in figure 4.3.

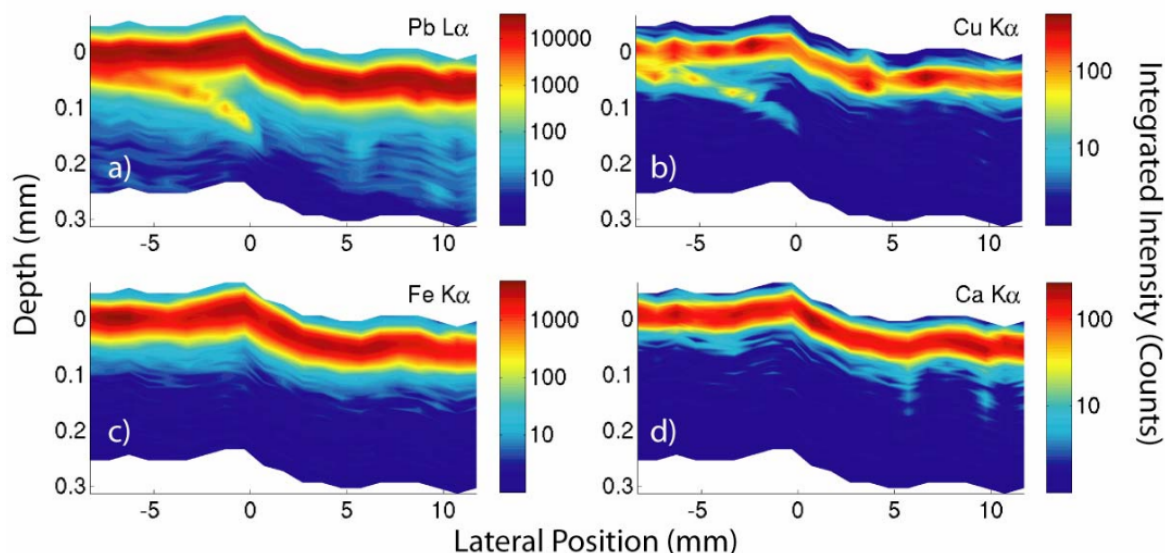


Figure 4.3: Virtual cross sections of David Teniers's *The Armorer's Shop* with scales indicating logarithmic fluorescent intensity for four key elements.

The development of mobile devices has broadened the scope of research possible with this XRF setup [26], [27]. However, dwell times of multiple seconds are required for depth resolutions of 10 μm in synchrotron facilities, and even several tens of seconds for depth resolutions of 40 μm using mobile X-ray tube-based instruments [28]. As a result, typically a point analysis is conducted to reduce scan durations. This has shown to be a good substitution for removal of paint cross-sections to analyze the layer structure of paintings [29], but it is not a practical method for investigating the composition of an entire painting. In order to study the global structure of a small painting, scan times would be far too long to be considered practical.

4.2.2. THz TIME DOMAIN SPECTROSCOPIC IMAGING

THz Time Domain spectroscopic (THz-TDS) imaging has been an important non-destructive technique in such fields as food safety, biomedical engineering, security screening, communication, medical imaging, and pharmaceutical control [30]. THz radiation lies between the infrared and microwave regions (frequency range about 0.1-10 THz) and can be safely used on art and archeological artifacts. Terahertz technology was successfully implemented as a tool for dendrochronology in 1998 by Koch et. al [31].

Since its discovery, THz-TDS has been used to examine the wooden supports of panel paintings by several research groups [32], [33]. Fukunaga et. al examined *The Polittico di Badia* by Giotto di Bondone, a tempera painting on wooden panel and the altarpiece of the Badia Fiorentina church. They were able to reveal paint layer build-up and crack damage in the wooden support using THz-TDS

techniques [34].

Only within the last decade has the application extended more into examination of pieces of cultural heritage [35]. THz-TDS allows for non-invasive material identification using known terahertz spectral databases as well as 3D mapping of the interior of a specimen without subjecting it to any intrusive damage. While this technique has promise as a non-invasive method of investigation for paintings, there are presently fewer than a dozen designated research groups focusing on THz technologies as tools for conservation. A lack of collaboration between facilities that develop the THz-TDS equipment and facilities that research and house cultural heritage prevents the technology from seeing widespread use [36].

Continuous wave (CW) THz sources have been successful in establishing a visualization of hidden paint layers and have been growing in popularity due to the simplicity of the equipment, the relatively low cost, and the speed with which results may be obtained. However, while pulse imaging is able to provide multivariate information, CW THz imaging is only able to provide yield intensity data using a fixed source and a single detector [37].

4.2.3. SYNCHROTRON COMPUTED TOMOGRAPHY AND COMPUTED LAMINOGRAPHY

Computed Tomography (CT) has been used since the 1970s for medical imaging [38], but its usage has been limited in the context of paintings due to their geometric structure. XCT yields the most precise mathematical results when the object to be scanned is within the field of view of the detector system at all angles. To ensure this happens, the scanner rotates about a single axis. The path length of the radiation must not vary more than roughly an order of magnitude through any given point of the absorbing material. For paintings, this is an issue when the source-detector is perpendicular to the edge of the painting, as the entire length of the painting would need to be able to transmit radiation. To circumvent this issue, in 2008 Krug et. al [39] prepared a high-precision computer controlled stage (see figure 4.4) that enabled a test panel to be rotated 360 degrees at an offset angle through an X-ray beam during image acquisition.

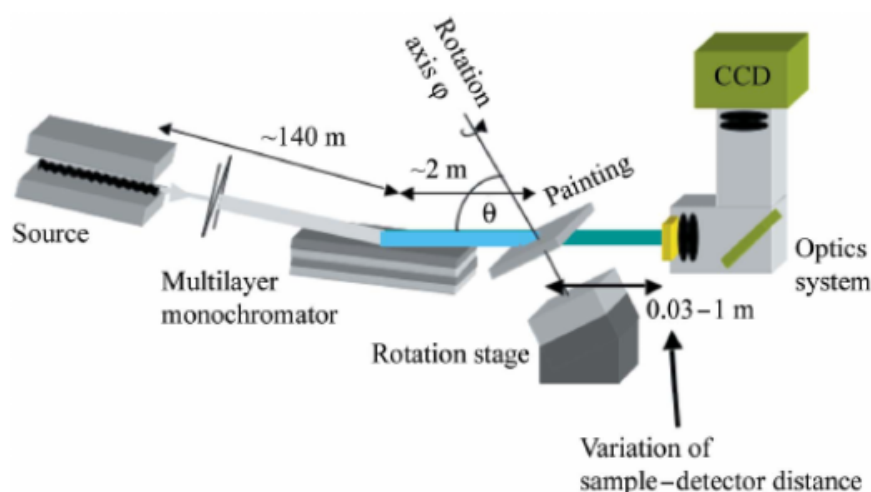


Figure 4.4: Schematic of the computed laminography setup utilized for investigation of a test panel by Krug et. al.

One drawback of this method lies in the fact that synchrotron radiation CT imaging of objects with lateral dimensions larger than the detector acceptance window will result in strong absorption of X-rays in the lateral directions. This is problematic because it results in artifacts for the digital

reconstructions of the images. Synchrotron Radiation Computed Laminography (SR-CL) was developed in order to overcome the difficulties encountered with synchrotron CT. Based on the principles of classical tomography and digital tomosynthesis [40], SR-CL utilizes monochromatic synchrotron radiation to reduce artifacts and gain resolution in imaging large flat objects. Krug's team utilized this method as well and as a result were able to obtain a visualization of the test panel structure, which is shown in figure 4.5.

One key advantage of these two scanning methods is the ability to understand the structure of objects that have organic elements within their composition.

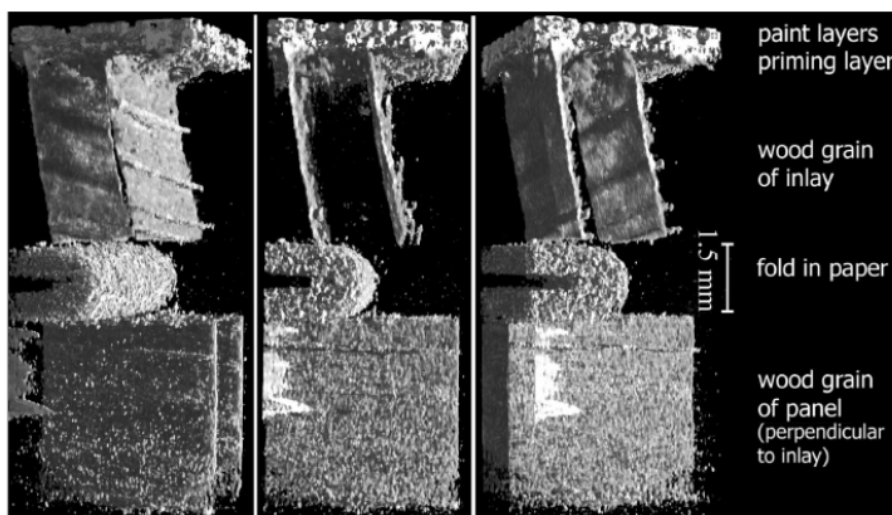


Figure 4.5: 3D rendering of test panel under different viewing angles, obtained by SR-CL by Krug et. al.

4.2.4. PUMP PROBE MICROSCOPY

Villafanna et. al [41] recently performed non-destructive analysis on Puccio Cappana's *The Crucifixion* using femtosecond pump-probe microscopy in order to obtain 3D images. Pump-Probe microscopy works by sending a series of ultrafast pulses (usually 0.2 ps in duration) to electronically excite ground state molecules into excited electronic states. To balance this excitation, the population distributions of the ground and excited electronic states rearrange to stabilize the energy of the system. A second pulse is administered to monitor these population redistributions.

Utilizing this technique, the research group was able to obtain a virtual cross-section of Puccio Cappana's *The Crucifixion* (figure 4.6 with information about the elements present as well as their specific location throughout the stratigraphy of the paint layers. However, a $55\ \mu\text{m} \times 545\ \mu\text{m}$ section of the painting had acquisition times of up to one hour, which would be prohibitive for the global analysis of a large painting. These lengthy acquisition times could potentially decrease in the future with detection sensitivity improvements, making it a more useful option for analysis or larger areas on paintings. There does not currently exist a pump-probe database for the most common pigment types, but efforts to produce one are being performed. In addition, some materials might not yield distinct pump-probe signals.

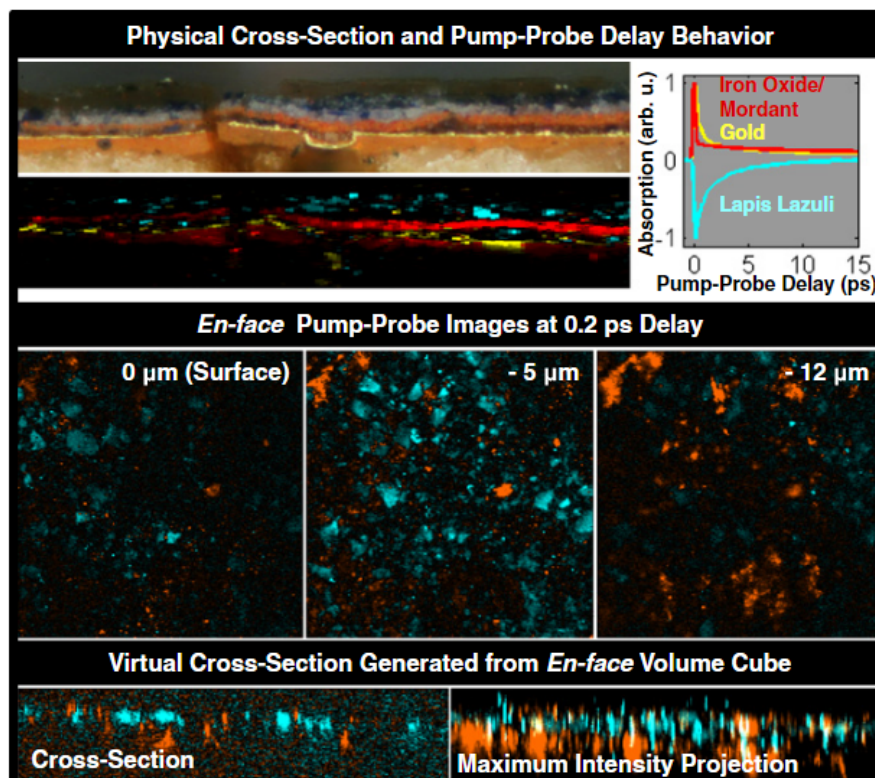


Figure 4.6: Investigation of the angels purple robe in Puccio Cappanas *The Crucifixion*. The top image shows a physical paint cross section, with a false-colored image below it showing the pump-probe delay behavior (cyan for lapis lazuli, red for the two iron-rich pigments above and below the gold layer, and yellow for gold). The pump-probe delay data set was acquired using 40 interpulse delays, 710/810 nm pump-probe, a total power of 1.5 mW, and dimensions 545 x 55 μm . Cumulative pump-probe traces of all identified pigments are shown in the graph. The dimensions of the virtual cross section at the bottom of the image are 185 x 50 μm .

5

IMAGE REGISTRATION

This chapter will first provide an overview of image registration, followed by an explanation of the mathematical concepts associated with automated registration procedures.

5.1. CHARACTERIZATION

Image registration is frequently used in the medical industry to map structural changes such as tumor growth, tissue losses, as well as for the study of disease [42]. It is also used for compiling and analyzing satellite images, photography applications, and *computer vision*. Computer vision is the science that aims to enable computers to gain a high level of understanding from digital images or videos. Through automatic extractions and analyses, the end goal is to derive useful information from a sequence of images. It utilizes the development of a theoretical and algorithmic basis to bring about an automatic visual understanding.

Image registration describes the complex process of determining a one-to-one mapping between the coordinates located in two separate spaces such that specific points in the these spaces that correspond to the same location in an object are mapped to one another. More simply stated, it involves a transformation of different data sets into one coordinate system. Utilizing computer vision, it is possible to perform complicated image registration procedures faster and with higher accuracy than is possible with manual techniques.

5.2. AUTOMATIC VERSUS INTERACTIVE METHODS

Image registration techniques can be categorized according to the level of automation that is used. There are four classifications of registration based upon methods that have been developed:

- Manual: this method utilizes interactive tools and software to manually align images to one another
- Interactive: The user still guides the registration process, however key operations are performed to reduce user error
- Semi-automatic: Registration steps are performed automatically, however the user verifies the accuracy.

- Fully automatic: All registration is performed automatically, no user input is required

Registration methods may be classified based on the level of automation they provide. Manual, interactive, semi-automatic, and automatic methods have been developed. Manual methods provide tools to align the images manually. Interactive methods reduce user bias by performing certain key operations automatically while still relying on the user to guide the registration. Semi-automatic methods perform more of the registration steps automatically but depend on the user to verify the correctness of a registration. Automatic methods do not allow any user interaction and perform all registration steps automatically.

5.3. HOMOGRAPHY IN COMPUTER VISION

A homography is a one-to-one correspondence that maps lines to lines by performing a projective mapping between two projection planes with the same center of projection. Therefore, two images of an object which both contain the same planar surface can be related through homography mapping. Computing a homography from two corresponding points in separate images of the same object is one of the most fundamental processes in computer vision. Using an estimated homography matrix, information about the translations of the device capturing the visual images can be extracted.

Mathematically speaking, a homography can be represented as a 3 x 3 transformation matrix in homogeneous coordinates that maps a pixel coordinate before transformation to a pixel coordinate after transformation. We denote the coordinates of a pixel before transformation as $\mathbf{x} = (x, y)$ and the coordinates after transformation as $\mathbf{x}' = (x', y')$. The action of the homography is represented compactly by utilizing homogeneous coordinates, in which the two-dimensional point \mathbf{x} is extended to a three-dimensional point $\mathbf{x}_h = (x, y, 1)$, following which the action of the homography is computed as a matrix multiplication by a 3 x 3 homography matrix \mathbf{H} , followed by a normalization of the resulting vector so that its z -coordinate is again unity. Thus, we first have

$$\mathbf{x}_h'' = \mathbf{H}\mathbf{x}_h$$

$$\begin{bmatrix} x'' \\ y'' \\ z'' \end{bmatrix} = \begin{bmatrix} H_{11} & H_{12} & H_{13} \\ H_{21} & H_{22} & H_{23} \\ H_{31} & H_{32} & 1 \end{bmatrix} \begin{bmatrix} x \\ y \\ 1 \end{bmatrix}$$

following which \mathbf{x}_h'' is normalized by dividing by its z -component so that it is again unity:

$$\mathbf{x}_h' = \frac{\mathbf{x}_h''}{z''} = \begin{bmatrix} x''/z'' \\ y''/z'' \\ 1 \end{bmatrix}.$$

Written out in component form, we thus finally have that

$$x' = \frac{H_{11}x + H_{12}y + H_{13}}{H_{31}x + H_{32}y + 1}$$

$$y' = \frac{H_{21}x + H_{22}y + H_{23}}{H_{31}x + H_{32}y + 1}$$

It can be seen that in the special case where $H_{31} = H_{32} = 0$, this is just an affine transformation encoding rotation, scale, translation, and skew. H_{31} and H_{32} are associated with perspective effects due to rotation of the camera (scanner) about its horizontal and vertical axes.

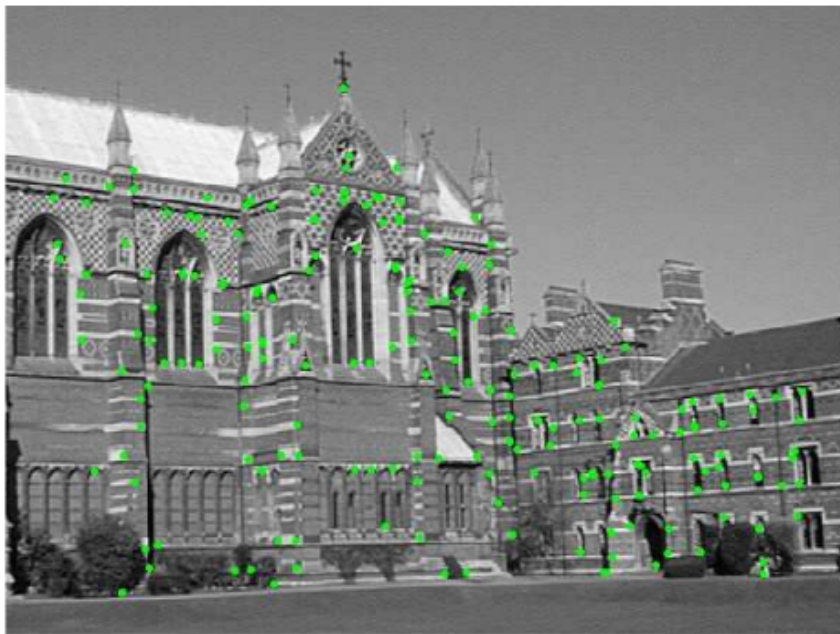
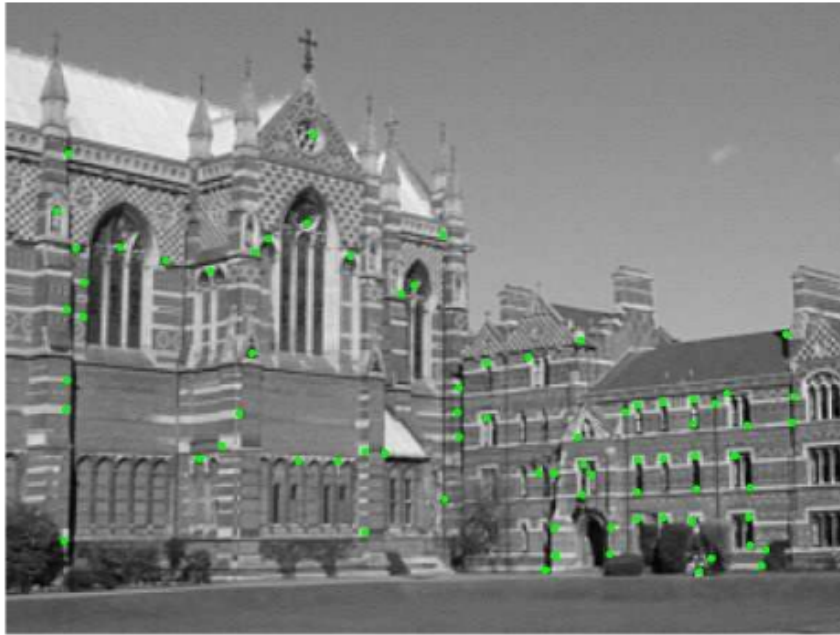


Figure 5.1: Example of preparation process for registration: The green dots indicate user dictated points that correspond the same place in both images. In this case, the user deliberately marked several points in the second image that were not marked in the first.

5.4. RANDOM SAMPLE CONSENSUS

To compute a homography, a direct linear transformation is performed using four or more point-correspondences between the images. These point-correspondences can be established automati-

cally by first locating key points between both images and representing them with a *descriptor*, and then comparing the descriptors. The resulting sets of point-correspondence pairs typically contain several incorrect correspondences, however. The Random Sample Consensus (RANSAC) algorithm is a robust iterative method for estimating the parameters of a mathematical model when there are outliers residing within the data sets. Correct data points are assumed to have a correlation while outlier data points are assumed to be random and therefore unusable. The RANSAC algorithm is frequently used in computer vision for homography estimation in the stitching and registration of two images of the same object.

The image transformations that are calculated using the RANSAC algorithm utilize a RANSAC loop, which is executed through the following steps:

1. Randomly select a *seed group* N_{sample} of point-correspondences to base the transformation estimate on. For homography estimations N_{sample} must be greater than or equal to four.
2. Compute the transformation from this seed group, i.e. estimate the parameters of the model from these samples.
3. Count the number c of inliers among the n data samples given the model parameters, using a threshold σ on residual error.
4. If the number in inliers is sufficiently large, compute the least-squares estimate of the transformation on all of the inlier data points.

The threshold σ is a critical parameter and ultimately determines how many inliers are considered in the homography estimations. If the value of σ is chosen as too large, outliers might be classified as inliers, thereby yielding a model with poor precision. Conversely, if σ is chosen as too small, inliers might be categorized as outliers, therefore causing them to be ignored.

Figures 5.1 and 5.2 graphically show the results of implementing a RANSAC loop for image registration.

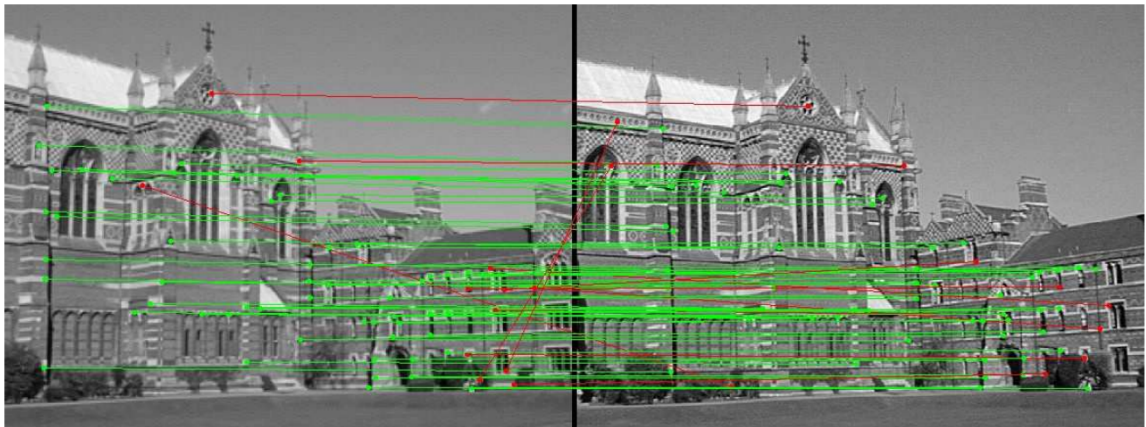


Figure 5.2: Example of results obtained from performing a RANSAC loop: the green lines represent inliers, while the red lines represent outliers. Positions that were not marked in the first image will be classified as outliers.

6

EXPERIMENTATION METHODOLOGY

This chapter discusses the experimental procedures used for addressing the primary goal of this research: to analyze the subsurface topography of hidden paint layers. A description of the test sample construction as well as the technical specifications and settings for the equipment used will be explained in detail.

6.1. SAMPLE PREPARATION

The ideal test case for the scope of this research is a painting constructed using impasto techniques which result in depth variations substantial enough to create a visible topography across individual paint layers. Due to the logistical constraints of experimenting with a piece of cultural heritage, it was necessary to prepare a mock-up sample for testing.

A simplified test case was constructed by first applying a (1-3 mm thick) 3 x 4 cm layer of lead white paint to the support, followed by a thick layer of calcium bone black paint applied directly on top of the lead white layer. The rationale for this sequence lies in the fact that Ca is a much lower Z element than Pb ($Z = 20$ versus $Z = 82$, respectively) and thus will not extensively hinder XRF radiation from escaping the sample and reaching the detector. It must be noted, therefore, that a reversal in the paint layer ordering would impact the results gathered in this research. Both paint layers were applied using impasto techniques with pronounced surface features ranging up to 3 mm from the support base. Each layer was allowed ample time for drying after application in order to avoid any volume and hence surface texture changes of the paints after scanning was performed.

The support for the painting sample was selected as a 12 x 9 cm piece of GLARE fiber metal laminate composite material, chosen for its rigidity and flat, even surface. The lead white paint layer is shown in figure 6.1 to the left of the finished sample with bone black paint applied over the lead white layer.

6.2. MOUNT DESIGN

The requirements for the sample mount included the ability to rotate the sample by 90 degrees while maintaining the distance from the tip of the scan head to the painting support. A metal alloy telescoping microphone stand was selected for sturdiness and the ability to extend up to heights capable of reaching the XRF scan head. The suspension boom of the stand was affixed with clamp holders that enabled rotation of the test sample in the x , y , and z planes via a bolt affixed to the back



Figure 6.1: On the left, the layer of lead white paint on GLARE substrate. On the right, the finished sample with bone black applied over the lead white paint layer.

of the support. A picture of the setup is shown in figure 6.2.

6.3. SURFACE CHARACTERIZATION

Since the ultimate goal of this research is to achieve topographical height information obtained from XRF scans, it was first necessary to extract quantitative data from the sample as a reference for comparison. This was obtained by performing 3D optical microscope scans first on the lead white paint layer after it was applied, and then afterwards when the calcium bone black layer was added on top, in order to establish a ground truth for the thicknesses of both paint layers.

A Keyence VHX-5000 digital microscope with a Keyence Multi-Scan Z20 lens set to 150x magnification was used to obtain high depth of field measurements across the sample. It uses technology that implements best focus data for each pixel to allow for clear, fully focused images to be observed and recorded. A high resolution image is obtained with single-wavelength light and an HDR function. These two mechanisms enable high resolution and high contrast observation. A fully focused image of each paint layer scan was constructed as the software compiled the images taken from a range of focal planes varying by increments on the μm scale. The focal plane data was then used to create a 3D model of both applied paint layers. Differential interference contrast and polarized light microscopy exposed the features, enabling a detailed visualization of the surface. Once the 3D models were created from the gathered images, the relevant data acquired by the VHX software enabled calculation of the profile and height of the paint layers across the entire sample.

Figure 6.3 shows the 3D optical microscope scan of a section of the Pb containing paint layer before the subsequent Ca paint layer was applied over it, and figure 6.4 the same section of the finished paint sample with calcium bone black applied over the lead white layer. Once these 3D images have been created, data can be collected to calculate the profile, height, and volume for any area within the field-of-view. Colored scale bars that indicate height are displayed on the images. Using a subtractive analysis, the thickness of the Ca top layer of paint can be determined at each point on the sample using the data recorded by the VHX software. A thorough account of the processing techniques for the height data obtained from the optical microscope scans will be discussed in detail in chapter 6.



Figure 6.2: The sample mount was selected as a telescoping microscope stand with clamp holders for easy rotation of the sample on all axes.

6.4. ACQUISITION OF ELEMENTAL MAPS

A Bruker M6 Jetstream mobile M-XRF spectrometer was used for all XRF scans of the test sample. The M6 Jetstream features a scan head capable of moving across the surface of an object on a motorized X,Y frame which allows for a maximum travel range of 80 x 60 cm with a minimum step size of 10 μm . A minimum dwell time per pixel of 0.1 ms is possible, resulting in a maximum stage speed of 100mm/s. The metal box supporting the frame houses the detector electronics, the electronics for the motorized stage, and the high-voltage generator of the X-ray tube.

The measuring head of the spectrometer consists of a 30 W Rh-target micro-focus X-ray tube. For the test sample scans, a beam energy of 50 kV and current of 0.6 mA was used. To achieve optimal resolution, the spot size was chosen as 100 μm with a dwell time of 80 ms and a step size of 100 μm . The focal distance was selected to be 9 mm after performing a set of test runs and choosing the distance that resulted in the highest resolution XRF images in terms of feature clarity. The measurement parameters chosen resulted in scan times of approximately three hours per scan, so in order

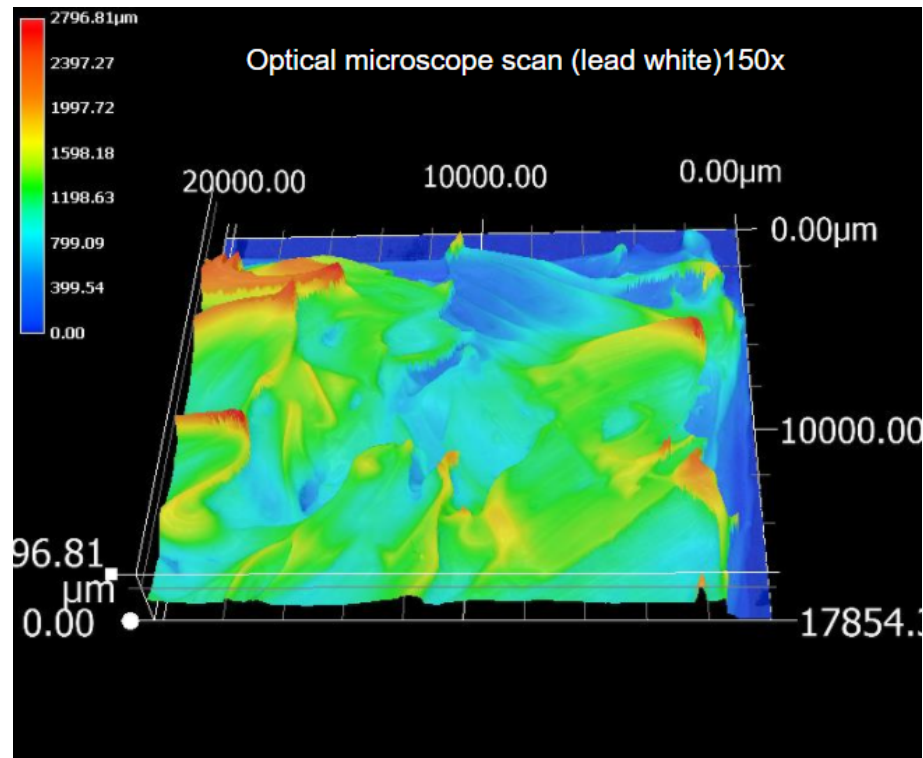


Figure 6.3: Optical microscope scan of the lead white base paint layer of the prepared sample

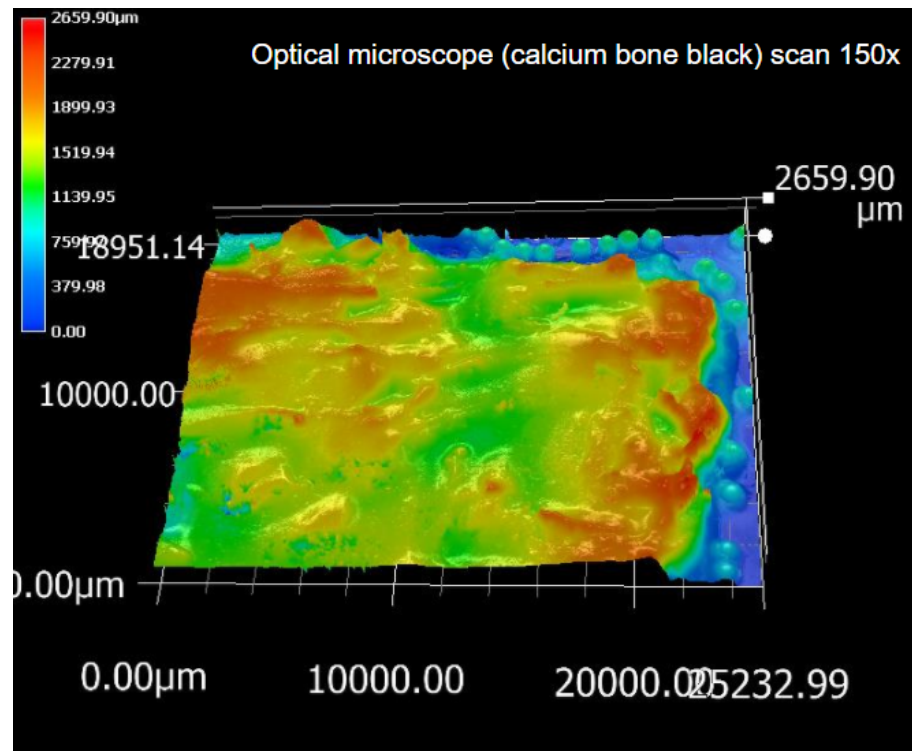


Figure 6.4: Optical microscope scan of the finished sample with bone black layer applied over the lead white paint layer

to ensure the focal distance remained constant,

As a result of the M6 Jetstream utilized for this research housing only one detector, it was nec-



Figure 6.5: Bruker M6 Jetstream mobile MA-XRF scanner

essary to simulate stereographic XRF scans obtained from four different angles. A primary concern for proper execution of the XRF scans was to ensure that there were minimal variations in tilt of the sample about its in-plane x - and y -axes. Even a tiny deviation can alter the apparent surface features of the paint layer topographies. To achieve a single self-consistent data set from the composite of the XRF images, it was necessary to ensure that the four corners of the painting support were equidistant to the flat portion of the plastic component at the front of the detector, with the X-ray beam normal to the test sample.

Upon completion of the XRF scans, the results were processed with PyMca software for accurate interpretation.

7

SAMPLE GEOMETRY CONSIDERATIONS

This chapter addresses some of the difficulties encountered while attempting to gather insights about the surface topography of hidden paint layers using MA-XRF, as well as for the registration processes used in this research. Section 7.1 discusses how to interpret stratigraphy from XRF maps, section 7.2 provides background on visual perspective, and section 7.3 explains the implications of the detector and source beam setup.

7.1. DETERMINATION OF HIDDEN PAINT LAYER ELEMENTAL COMPOSITION

When a painting is investigated using XRF, pigments from the surface painting as well as those from any hidden paint layers are obtained in 2D maps. There is no indication of the stratigraphy of the paint layers, so an estimation must be made if there is no supporting information about the sequence of the paint layers (for example with a physical paint cross-section). We are only interested in utilizing XRF to gain an understanding of the surface structure of *hidden* paint layers for this research, so a distinction must be made between XRF data of the surface paint layers and those of interest which lie beneath the surface. Human inspection is a key component of this process; by referencing databases such as the Fiber Optics Reflectance Spectra (FORS) [43] a classification can be obtained by referencing the 54 common pigments used in historical paintings. By comparing the visible painting with the individual elemental XRF images obtained through scans, a cross-reference of the pigment database can reasonably provide the necessary insight to determine whether the XRF visualized elements are part of the surface painting or underlying layers.

In the case of the constructed test sample, it was known that lead white was used for the hidden layer. However, it was evident that this was the case for the lead XRF images based upon a visual examination of the sample, as only the calcium bone black layer was observable with the naked eye. This reasoning can also be applied to actual paintings with hidden compositions if elements observed via XRF are not present in the pigments used for the surface painting.

7.2. CHANGES IN PERSPECTIVE OF SAMPLE FEATURES

There are two characteristic features of perspective when viewing an object: objects are smaller as their distance from the observer grows, and they are subject to foreshortening, which means the objects dimensions along the line of sight are shorter than the dimensions perpendicular to the line of sight. The photographs of the statue in figure 7.1 provide an example of how the observed

dimensions of an object change as the viewer changes position. The size and shape of the features appear differently as the observer photographs the statue from various angles.



Figure 7.1: *The Scourge* by Lazzaro Morelli photographed from three different angles. Changes in perspective result in foreshortening of the statues features.

The rotation of the test sample can be thought of in a similar context: each rotation simulated detector movement. As in photography, this causes changes to the way the surface features are visually perceived. As the sample is rotated, the appearance of the features change as a result of their relative distance from the detector. This presents an issue for one of the key tasks at hand: creating a composite image of the four XRF images. A basis image is necessary for comparison to the optical microscope scans, however the feature-points in the test sample XRF images cannot easily be registered to one another, since they appear to change from one scan to the next. To circumvent this issue, steel ball bearings 1 mm in diameter were positioned around the edges of the calcium paint layer and affixed to the substrate to provide smaller features that would be less subject to drastic perspective changes.

7.3. TARGET GEOMETRY

The geometry of the experimental setup plays an important role in X-ray scatter and detection. It will also have an effect on how the physical aspects of the sample will be preferentially illuminated or cast into shadow. The M6 Jetstream used for this research features an X-ray source that irradiates the sample with a beam normal to the surface and a detector angle of 45 degrees relative to the source beam. This setup has the advantage of an optimal horizontal beam size and potentially less shadowing in the XRF images from features in the sample. However, even with this advantageous setup, shadowing and illumination are not avoidable.

To visualize what this looks like in terms of the test sample, refer to the XRF image in figure 7.2. The circles indicate locations on the surface of the Pb paint layer that were particularly prone to this effect. The green circles highlight areas of strong signal intensity, and therefore reduced shielding effects caused by overhung features. The red circles show the resulting shadows these features create

through the effects of shielding.

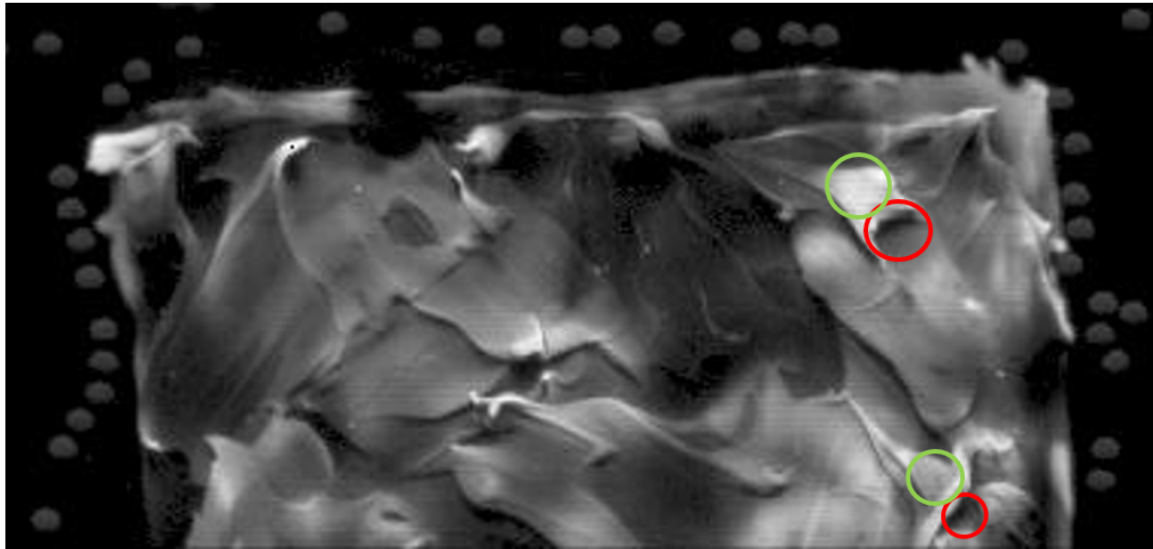


Figure 7.2: XRF image of hidden Pb paint layer with noticeable effects of shielding. Red circles highlight shadowing effects caused by shielding while green circles highlight areas of high lead intensity corresponding to the same feature at a different angle relative to the detector.

It is important to note that this would not be as problematic an issue in an XRF setup with four detectors. The XRF image brightness corresponding to the captured XRF fluorescence from an element, if measured simultaneously from four different angles, would simulate a feature being lit from all sides and thereby reduce shadowing effects.

8

DATA PROCESSING AND IMAGE REGISTRATION

This chapter presents the data processing methods that were employed to realize the ultimate goal of this research: Creating digital 3D visualizations of the topography of hidden paint layers.

8.1. OVERVIEW

As described earlier, the XRF scans simulated four different detector angles through rotation of the test sample in the plane normal to the source beam. To account for the shielding of signal from the detector that may be present at any given detector orientation, we must first perform registration among the four scans to bring them into precise alignment. For this work, we utilized the Pb-L XRF maps since the concealed paint layer was painted with lead white. Once the four separate scans are brought into alignment, a hybrid scan image can be constructed in which the shadowing artifacts are reduced. The first step for generating this hybrid image is to determine the approximate geometric transformation that is needed to bring the four stacked XRF images into correspondence with one another by transforming the scan images into a single coordinate system. The open-source vector graphics editor software Inkscape was used for this manual registration process. As opposed to raster graphics editors such as Photoshop, Inkscape stores graphics in a *scalable vector graphics* (SVG) format file (.svg) which contains mathematical descriptions of affine transformations. It utilizes a resolution-independent description of the actual shapes and objects that are displayed in an image and a rasterization engine which subsequently uses this information to determine how to plot each feature at any resolution or zoom level. In contrast to raster, or "bitmap" graphics, SVG is not bound to a specific resolution because it does not store an image as a grid of pixels. An x, y scale and six degrees of freedom allow for rotating, skewing, translating, scaling, shifting, and stretching an image with no impact on the images resolution. The resulting .svg file contains the information on how the registered images should be moved from their original position.

8.2. ADDITIONAL SAMPLE PREPARATION

As discussed in chapter 7, image perspective is an important aspect of the registration process that can present difficulties. Given that the test sample had pronounced surface features that appeared different in each scan as a result of the changing detector angles, it was not possible to precisely register the images to one another with only the Pb features. To circumvent this issue, 1 mm diam-

eter stainless steel ball bearings were affixed to the substrate at the perimeter of the surface paint layer to provide additional features that could be used to align the images. It is important that the features be relatively small and at widely spaced positions across the sample to ensure proper image alignment and minimal transformation error.

8.3. INKSCAPE REGISTRATION

Out of the four XRF maps of the element to be analyzed, the one with the most ideal geometric parameters is selected to be the "anchor" image. To simplify the following discussion, we will refer to the four scans as images *A* (first scan) *B* (90 degree rotation), *C* (180 degree rotation), and *D* (270 degree rotation). One at a time, *B*, *C*, and *D* are superimposed onto the anchor image *A* in order to line up the coinciding features. To accomplish this, the transparency of the superimposed image is increased until the features of the anchor image are clearly visible through the superimposed image. Local transformations of the overlaid image are manually performed, including translation, rotation, and, if needed, anisotropic scaling and skewing to achieve the best visual match between the overlaid image and the anchor image. Throughout the process, image *A* is left in its initial position, scale, and orientation, i.e., its initial position is assumed to be correct. After images *B*, *C*, and *D* are approximately aligned to image *A*, the resulting stack of four images is saved into an .svg file. This is the starting point for the more complex automated registration process, which will be discussed in the following sections. It should be noted that Inkscape only allows for the specification of affine transformations and that it therefore cannot accommodate the perspective tilts that can be described with a full homography.

8.3.1. AUTOMATED REGISTRATION OF ELEMENTAL XRF MAPS

The auto-registration process involves optimizing the alignment of the paired images obtained from the manual registration performed in Inkscape using the previously described RANSAC method. The first step for performing the optimization process involves deconstructing the paired images into a grid of multiple "tiles". By dividing the images into many smaller images, it is possible to compute the feature mismatch in the local coordinate system as opposed to the global coordinate system. Each pair of tiles is then individually considered in the auto-registration process. The next section will detail the steps taken to perform this optimization.

8.4. OPTIMIZATION THROUGH CORRELATION ANALYSIS

First, the Inkscape data is uploaded into the Python environment and a code module reads the mathematical descriptions contained in the SVG files. A correlation analysis is executed through an exhaustive comparison of each pair of images for which matches are sought. To establish a match between the pairwise images, close proximity descriptors are sought in the high-dimensional descriptor space. It would be computationally prohibitive to compare every descriptor in the images, so instead an adaptive algorithm is used to hasten the search for pairs of matching descriptors.

The correlation analysis is performed by isolating two paired image tiles at a time and shifting them through all possible vertical and horizontal overlaps, looking at all relative placements of the top and bottom tile. The goal of this step is to find the geometric parameters which minimize the mismatch between the feature points that are known to match. This mismatch is described using an error metric which will be minimized. These shifts are conducted until the best possible match is found between each set of tiles. A simplified schematic of this process is displayed in 8.1.

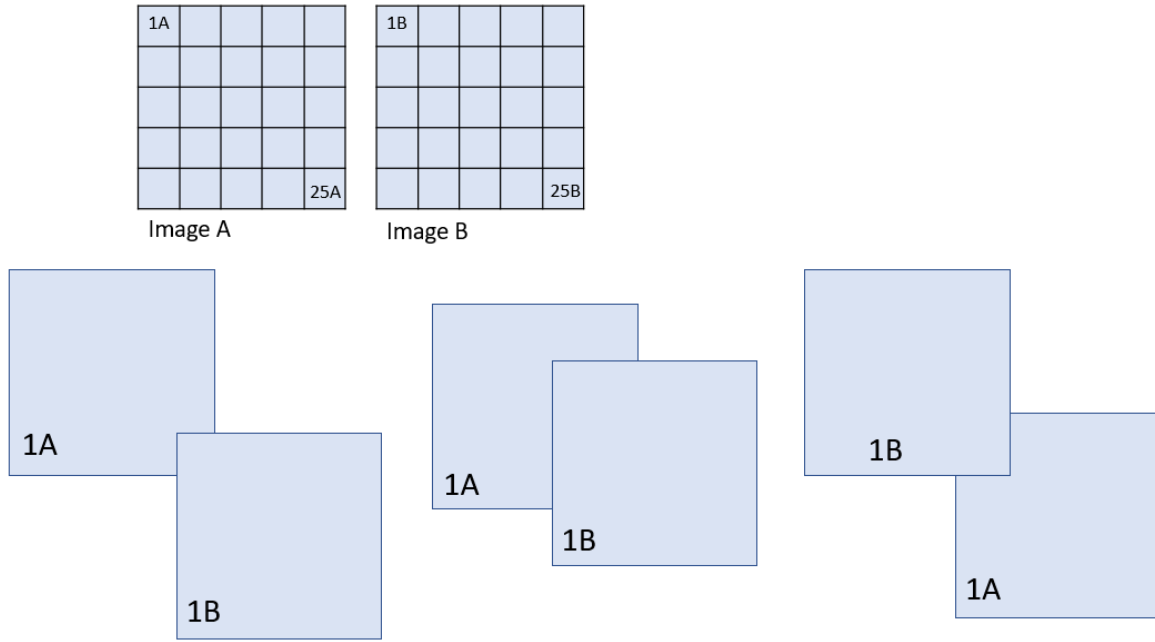


Figure 8.1: Graphical overview of the XRF scans cut into tiles, which be subsequently paired and translated relative to one another until the best possible match is obtained.

The two 5 x 5 grids at the top of the figure represent XRF scanned images *A* and *B* divided into 25 individual image tiles for reasons of simplicity. The computer shifts tile 1B over tile 1A into all possible translations, starting out with barely any overlap at all and leading up to almost total overlap of the tiles. For each relative shift, the similarity between the two image tiles amounts to their overlapping parts. The goal is to locate the positioning that gives the strongest similarity between the two tiles that are being operated on by measuring the x , y shifts that bring them into the closest correlation with one another.

The result of this tile-wise correlation analysis is a set of translational offsets associated with tile centers spread across the images. We denote the observed shift for tile pair k as $(\Delta x_k, \Delta y_k)$. This global pattern of local tile offsets is assumed to be modeled by a homography since the homography is the most general transformation associated with moving a camera relative to a planar imaged surface. The mathematical problem is thus to estimate the 8 parameters of the homography that would best describe the observed pattern of tilewise offsets. Given this homography, its inverse can be subsequently applied to the second image to place it into registration with the first image.

The fitting of the pattern of tilewise offsets with a homography is framed as a numerical optimization problem. Given some homography matrix \mathbf{H} (with 8 scalar parameters H_{ij}), the homography applied to the coordinates of the tile centers produces a new set of transformed tile centers. The translation between the original tile center coordinates and the homography-transformed tile center coordinates is a predicted local correlation shift for tile k of $(\Delta x_k^p, \Delta y_k^p)$. The sum of squared differences between model-predicted and observed tile offsets is a measure of the error E of the model:

$$E = \sum_k (\Delta x_k - \Delta x_k^p)^2 + (\Delta y_k - \Delta y_k^p)^2$$

The best homography is then the one minimizing this overall error, thereby necessitating the use of a numerical optimization process. We utilize the Levenberg-Marquardt algorithm [44] for non-linear least-squares problems with the added RANSAC step which only retains feature points with mismatches of less than one pixel in the image-local coordinate system. Complex translations are

inferred by looking at the individual movements and an overall picture of the required motions can be obtained. Each of the Pb XRF images acquired after consecutive 90 degree sample rotations were paired with the Pb XRF image from the first XRF scan (the so-called "anchor" image). Each pair was then divided into hundreds of tiles, to provide smaller regions of comparison between the two images in question. By performing the transformations previously described, a best guess for how to translate tile 1B to match 1A as closely as possible is achieved. By observing these smaller local shifts, an estimation can be made as to what is necessary to bring them into correlation with one another. The specifications of the source code instructed the operation to be performed three times in a row for each paired tile. Starting with 1B on 1A, then 1B' on 1A, B1" on 1A...nB" on nA. These transformations are then repeated with 1C on 1A... and then 1D on 1A until nD" on nA is executed. Using three passes for each pair of tiles, it was possible to achieve sub-pixel registration accuracy (0.2 pixels) for each pair of transformed tiles through all four Pb XRF images. Figure 8.2 shows a simplified schematic of the process.

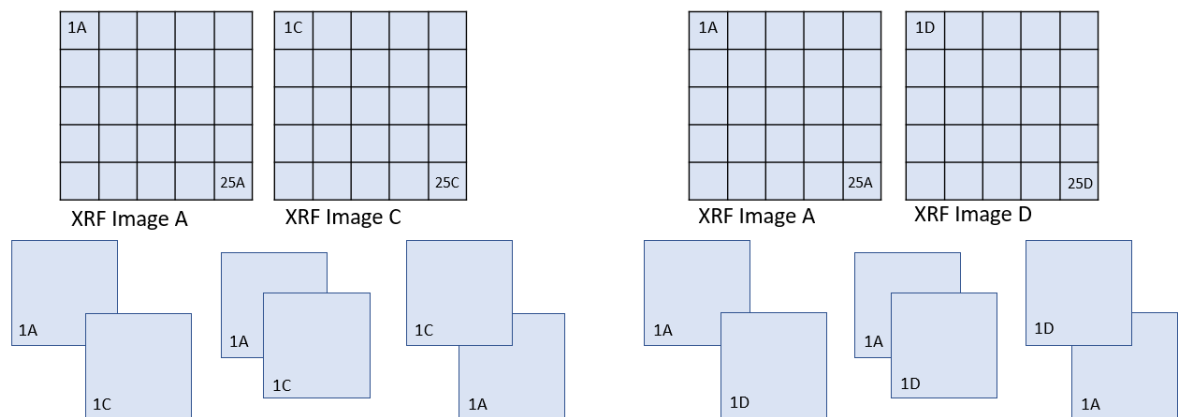


Figure 8.2: Continuation with images C and D

This near-perfect registration among all of the paired tiles then enabled a global transformation of the four stacked Pb XRF images to be inferred. The hybrid image is then observed to ensure that the results of the registration are sensible. If there is poor geometric fit or large mismatch between the images, the registration is not considered successful.

8.5. PRODUCING HYBRID ELEMENTAL INTENSITY IMAGE

Once a near-perfectly registered hybrid image of the four XRF maps was obtained, the next goal was to attempt to reduce the visual effects from Ca shielding in the image. As discussed in 3, for each pixel in an XRF image, the brightness can be interpreted as the strength of the signal for the element being observed. Pixels with a lower brightness signify a lower signal intensity. This can also be interpreted to mean that there is a greater possibility shielding was more prevalent. In a high resolution XRF image of a paint layer with clear surface layer variations, this shielding is visually perceived as shadowing from the surface features of the paint layer.

In this case, we have four Pb XRF images with correlating pixels registered to one another. By taking the brightest pixel of the four, we are selecting that which corresponds to the strongest Pb signal. Considering each pixel is registered to the corresponding pixels in the other three XRF maps, the lowest signal of the four indicates not an absence of lead, but rather a pixel corresponding to a point on the paint layer surface located on an angle that was shielded from the detector. By eliminat-

ing the three pixels with the lowest brightness from each stack, we are selecting the pixel that was least affected by shielding, ultimately enabling registration into a hybrid XRF image with minimized shadowing and maximized visual information regarding the surface features. Through this process, we have attempted to use four XRF scans to infer pixel by pixel whether the Pb intensity (or lack thereof) is a result of shielding, or simply a lack of Pb presence. The result is an optimistic hybrid Pb XRF image with a reduction in artifacts created by shadowing effects.

Each stack of four pixels across the entire hybrid XRF image was considered, and the brightest pixel in each stack of millions of stacked pixels was selected in order to compose the final rendered hybrid image.

8.6. REGISTRATION OF XRF IMAGE TO HEIGHT MAP

The ultimate goal of this research is to determine if XRF scans obtained with multiple detector angles can provide us with information about the topography of hidden paint layers. The steps taken up to this point facilitate the creation of a composite image of four elemental XRF maps scanned with different detector angles with peak intensity extraction. In order to make a correlation between the XRF images and the quantitative data obtained from optical microscope scans, registration of the composite peak intensity Pb XRF image to the optical microscope height map of the Pb paint layer is then necessary. The same process as described in the preceding sections with additional steps added can be used to accomplish this.

For the registration of the Pb XRF images to each other, it was not necessary to perform any operations that changed the dimensions of the images in any way. Anotherwords: no skewing, stretching, or similar actions were needed. Simple rotations or shifts were all that was required due to the identical scale of each XRF image. However, the optical scan was obtained with different equipment, therefore the height map could not be superimposed onto the XRF map (or vice versa) using the same transformations as before.

The resolution of the optical height scans far exceeded the composite Pb XRF image, so a decision was made to retain the high quality of the 3D optical microscope image and transform the XRF images instead. Following the same procedure as before, the images were uploaded to Inkscape for manual registration. The composite Pb XRF image was superimposed onto the 3D height map, then the transparency of the XRF image was increased until the features of the 3D height map could be seen through it. The XRF image was then manually registered to the height map using stretches, shifts, and rotations until the feature-points of the two images were in correspondence with one another.

The computer was then instructed to perform the same auto-registration procedure that was described in section 8.4, this time with the SVG data file of the Inkscape registered composite Pb XRF image and optical microscope 3D height map. Upon completion of this final correlation analysis, we are left with a pair of images that are perfectly registered with sub-pixel precision. These images can then be compared to one another to determine whether there is a strong correlation between the height information obtained with the microscope and the Pb intensity information obtained via XRF scanning.

9

RESULTS

This chapter presents the results of the data processing and image registration procedures discussed in chapter 8. Section 9.1 provides the preliminary XRF images obtained with scanning, and section 9.2 shows the results of the ultimate research goal: the ability to visualize the topography of a hidden paint layer using mobile XRF.

9.1. PRELIMINARY XRF SCANS

Figure 9.1 shows the XRF images for the calcium bone black surface paint layer and the hidden lead white paint layer. The pair of XRF images on the top right were obtained from the first scan, then moving clockwise through the images each pair of XRF images was obtained through scanning after consecutive 90 degree sample rotations. The detector angle measured 45 degrees from the test sample support, with the incident source beam normal to the sample surface. It can be seen in these images that depending on the detector angle relative to the surface, the effects of shielding have a varied effect on the size and location of shadows that are present. This provides evidence that using alternating detector geometries for a sample with pronounced features can have a measured effect on the recorded intensity of the X-ray fluorescence for each location on a painting. In a situation where scanning with four detectors simultaneously is not possible, these shadows can be used with the aforementioned data processing methods to hypothesize the physical topography with promising results.

9.2. REGISTRATION OF XRF MAPS TO HEIGHT MAPS

After registering the Pb XRF images obtained through the four consecutive scans, and then neglecting all but the brightest pixel in each stack of four registered pixels across the entire hybrid XRF image using the process described in section 8.5, we were successfully able to create an optimized hybrid Pb XRF image that hypothesizes the surface contours of the hidden Pb paint layer. This image could then subsequently be registered to the quantitative height map.

Figure 9.2 shows the final registered images of the optical microscope scanned Pb paint layer to the hybrid MA-XRF image with the stacked pixel intensity optimization. For the height map, brightness increases with the height of the features. Correspondingly, in the XRF image the brightness increases with Pb intensity. The brightest areas are an indication that Ca shielding was not as prevalent, which essentially translates to closer surface proximity in this case.

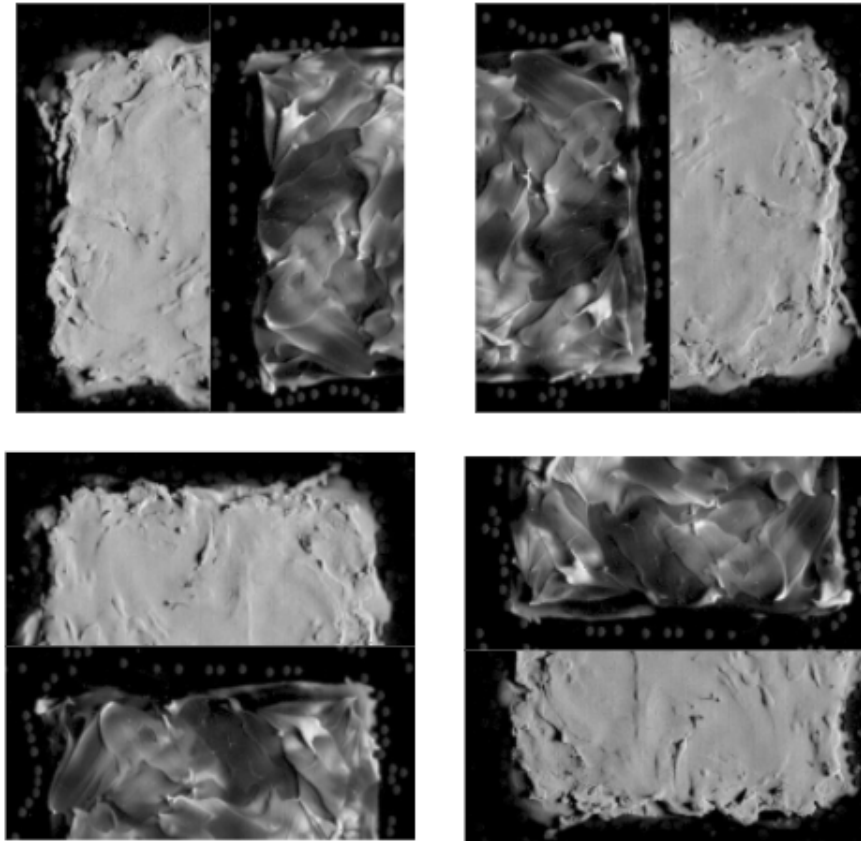


Figure 9.1: XRF images for Pb and Ca. The images show the scans performed after 90 degree sample rotations that simulated multiple detector angles. Since the detector position is fixed, each rotation of the sample enables the detector to collect data from a different angle

It is evident that there is a strong correlation between the brightness of corresponding features in the two images. This is an indication that visible features with a high Pb intensity in the XRF image can be interpreted as surface features with elevated height. There are, however, some obvious discrepancies between the two images: for example, refer to figure 9.3. The selected areas are features that are much brighter in the XRF image than in the height map image, or vice versa. By closely observing these locations, it is apparent that there is a slight overhang of the paint peaks. This additional paint in the line of sight of the detector results in more Pb observation by the detector than height observation by the microscope. Therefore, it must be taken into consideration that the height as seen by the microscope will not always correspond to the thickness of the Pb as seen by the detector when a complex topography exists. In the case of the feature that appears brighter in the microscope image, this is likely due to it being a very thin and relatively tall feature; it was not sufficiently thick enough in the vertical direction to cause ample Pb detection.

In addition to shielding, which the max-pixel brightness method aims to account for, there is also attenuation from several sources:

1. Inbound X-rays are attenuated through Ca
2. Inbound X-rays are attenuated through Pb to reach deeper Pb
3. Outbound fluorescent X-rays are attenuated through Ca
4. outbound fluorescent X-rays are attenuated through Pb

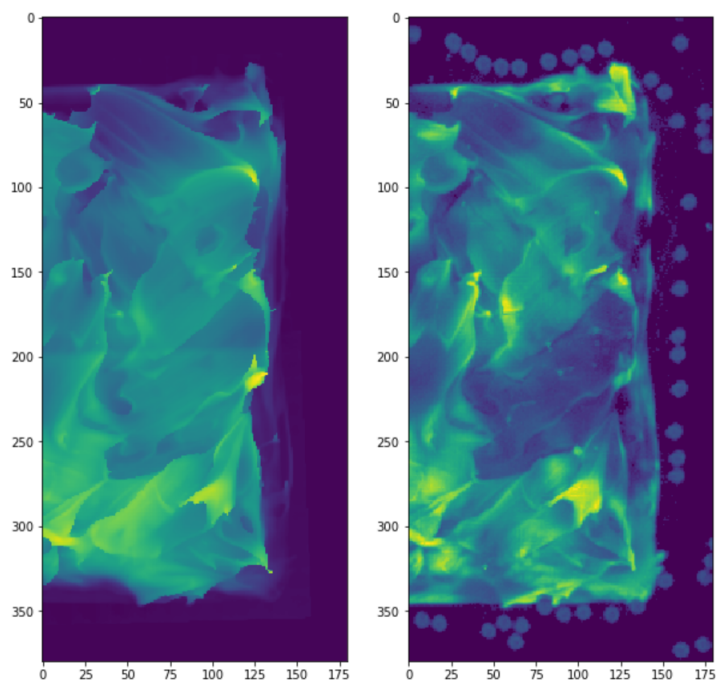


Figure 9.2: Pictured left is the height map for the lead white paint layer obtained with the optical microscope and on the right the MA-XRF image of the lead white paint layer. For the height map, brightness increases with height. For the hybrid XRF image, brightness increases with Pb intensity.

In order to make a more quantitative model, all of these factors must be taken into consideration.

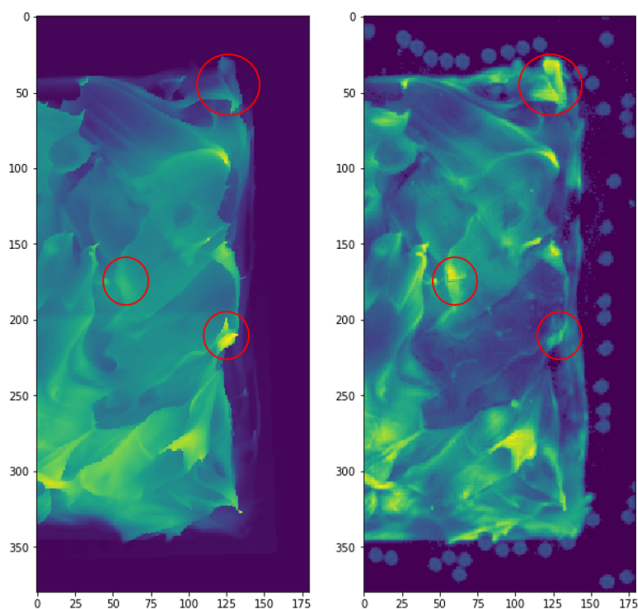


Figure 9.3: Corresponding features that do not appear to correlate in terms of height. These locations in the paint layer had overhanging surface features, which resulted in higher intensity readings in the XRF scans.

While this hybrid XRF image does not provide quantitative information about the ground truth thickness of the Pb paint layer, it does enable a visualization of the topography of a completely concealed paint layer. When compared to the height map, strong evidence of a correlation between

the Pb intensity and the actual height of the Pb paint layer can be seen.

10

DISCUSSION

10.1. REPRODUCIBILITY

There were certain limitations to the extent of experimentation that was possible for this research. Ideally, numerous test runs would have been executed for a broad array of test sample constructions. However, time and equipment restrictions limited the number and scope of test cases.

The painting sample that was analyzed for this thesis work constituted an ideal test case: lead is a heavy element that will produce a strong XRF signal. In addition to this, the calcium-rich bone black pigment will not absorb an abundant amount of the fluorescent X-rays emitted from the Pb atoms in the lead white paint layer. In an actual painting, the likelihood of this ideal succession of paint layer stratigraphy might not be as simple and straightforward. However, the results obtained in this research definitively show that it is possible to obtain a qualitative visual representation of the topography of hidden paint layers with the information obtained from traditional scanning MA-XRF.

There are currently no mobile scanning MA-XRF units equipped with four detectors, so for the time-being similar research will necessitate rotation of the object under investigation. This could present challenges for a historic painting; more in-depth considerations would need to be taken into account for the construction of a suitable mount for the painting. Paintings infrequently possess a perfectly flat support; particularly in the case of historic paintings linen canvas or wooden panels were used. Over time, moisture uptake and other deleterious environmental effects in wooden and canvas supports will cause warping. This will be problematic when scanning actual paintings, as they will not have a perfectly flat support (or surface) that can be used for measuring distance to the scan head. This will likely increase the error of the experimental results if conducted in the same manner as this thesis proposes.

Additionally, it is not possible to affix permanent markers to a painting to assist with the registration process. In the case of this research, registration to the microscope height map was possible once the hybrid max-brightness image was obtained; the features of the lead white paint layer were more well-defined once the effects of shielding were reduced. This could translate to other cases as well depending on the complexity of the interfacial topography.

The ideal setup would consist of a permanent stereographic setup, namely four (or more) detectors positioned around the source beam. Not only would this help to alleviate any difficulties associated with ensuring all scans are repeated at equal distances from the detector, it would also result in a drastic reduction in scan time length. Smaller step sizes and longer dwell times would be possible, which would increase the XRF image resolution.

10.2. FEATURE DETECTION IN XRF IMAGES AND SURFACE PAINTING

The value of understanding the topography of hidden paint layers for conservation and restoration purposes relies on the ability to correlate hidden features with specific locations on the painting. Humans have limited visual memory, which is problematic when attempting to locate the same point on two side by side images. To circumvent this issue, it is recommended that a digital curtain viewer is created in order to establish correspondence of the XRF images with the visible painting. Erdmann et. al [45] published research detailing the creation of this technology as applicable to paintings. An example of their curtain viewer technology used for Heronymous Bosch's *St. John the Baptist* is shown in figure 10.1.



Figure 10.1: Curtain viewer technology employed for Heronymous Bosch's *St. John the Baptist*. In curtain mode the division between the panes follows the mouse cursor

10.3. EXPERIMENTAL ERROR

As discussed in section 6.4, a primary concern for proper execution of the XRF scans was to ensure that there were minimal variations in tilt of the sample about its in-plane x - and y -axes. Originally, the plan was to construct a rotating mount that would be permanently affixed to a wall to ensure total stability and minimal variations on the z axis. However, the M6 Jetstream that was utilized for this research was simultaneously being used for scanning large paintings which required the unit's support to be switched out every week in order to adjust the height of the frame. As a result, a fixed wall mount was not practical. It was difficult to ensure that the sample corners were all perfectly equidistant and at the same distance from the detector for each scan with the setup that was used. This likely resulted in some error of measurement for the XRF scans, but it is not possible to quantify this error. It is assumed to be minimal based upon visual observations and physical measurements performed while setting up the experiments.

10.4. RECOMMENDATIONS

The results of this research have proven to be very promising for the extension of MA-XRF into being used for analyzing the 3D topography of hidden paint layers. As mentioned in section 10.1, an ideal

setup would consist of a source beam with four detectors mounted around it. Collaboration with a manufacturer of mobile MA-XRF spectrometers for the development of a prototype unit would facilitate a simpler procedure for data processing, and reduce the amount of time needed for scanning. Higher resolution scans could be obtained by increasing the dwell time per pixel and decreasing the step size while still benefiting from reduced scan times.

The test sample had a very simple construction with only two paint layers. A more elaborate mock-up sample with several different pigments of varying atomic weight should be investigated to determine whether this approach is practical for more complicated paint layer stratigraphies.

As discussed in section 9.2, attenuation of X-ray fluorescence is also a concern and should be taken into consideration in order to make a more quantitative model.

10.5. CONCLUSIONS

The primary goal of this research, to create digital 3D visualizations of the topography of hidden paint layers using non-destructive and well-established techniques, was achieved by using a mobile XRF spectrometer and a unique data processing approach. The following procedures were presented in this thesis:

1. *Chapter 8 describes the methods used for registering XRF images obtained with different detector geometries to one another and subsequently to a quantitative height map.*

First, manual registration using vector graphics editing software was performed. This was followed by an automated procedure using a ransac loop, which brought the four scanned XRF images together into a hybrid image with near perfect correlation. On a pixel by pixel basis across the hybrid XRF image, the brightest of the four in each stack of pixels was selected in order to reduce visible artifacts and enable the creation of a digital rendering of the topography of the hidden Pb paint layer.

2. *Chapter 9 displays the digital image results of the data processing methods that were employed.*

The hybrid Pb XRF image created using the techniques described in chapter 8 was successfully registered to the quantitative height map. A visual comparison can now be made between the two images, and a strong correlation is observed. The colouration in the height map is scaled to increase in brightness with height, and in the hybrid Pb XRF map to increase in brightness with recorded Pb intensity. For the XRF image, this intensity can be understood as features with the least amount of shielding, and therefore represents features closer to the painting surface, i.e. at higher elevation.

We have shown that it is possible to use MA-XRF to characterize the surface of a hidden paint layer with a straightforward approach using novel data fusion algorithms and visualization techniques. Using the techniques described in chapter 8, we were able to create a visualization of the topography of a hidden lead white paint layer using mobile MA-XRF scanning. Additional insights about paintings can be gained by utilizing mobile MA-XRF scanners that are currently housed in museums and research facilities to scan paintings in multiple orientations. However, mobile XRF units that are commonly used in museums today typically have a single detector, which limits the applicability of this method for larger paintings. Careful design of a motorized mount would assist in analyzing interfacial paint layer topographies for smaller to medium sized paintings using existing mobile XRF units.

This approach is not limited to paintings; any field of research that frequently uses XRF technology stands to benefit from the ability to gain knowledge about the substructure of materials using this technique.

BIBLIOGRAPHY

- [1] J. Dunnmon, S. Sobhani, M. Wu, R. Fahrig, and M. Ihme, *An investigation of internal flame structure in porous media combustion via x-ray computed tomography*, [Proceedings of the Combustion Institute](#) **36**, 4399 (2017).
- [2] W. D. Carlson, *Three-dimensional imaging of earth and planetary materials*, [Earth and Planetary Science Letters](#) **249**, 133 (2006).
- [3] W. Aburjaile and A. Mourao, *Development of a chest phantom for testing in computed tomography scans*, *Radiation Physics and Chemistry* (2017).
- [4] S. Zesch, S. Panzer, W. Rosendahl, J. W. Nance, S. O. Schönberg, and T. Henzler, *From first to latest imaging technology: Revisiting the first mummy investigated with x-ray in 1896 by using dual-source computed tomography*, [European Journal of Radiology Open](#) **3**, 172 (2016).
- [5] M. Faries, *Analytical capabilities of infrared reflectography: An art historian's perspective* (National Academies Press, 2005) pp. 87–104.
- [6] R. Mould, *A Century of X-rays and Radioactivity in Medicine*, 2nd ed. (Institute of Physics Publishing, 1995).
- [7] P. Dhamelincour, F. Wallart, M. Leclercq, A. T. N'Guyen, and D. O. Landon, *Laser raman molecular microprobe (mole)*, [Analytical Chemistry](#) **51**, 414A (1979).
- [8] I. M. Bell, R. J. Clark, and P. J. Gibbs, *Raman spectroscopic library of natural and synthetic pigments*, [Spectrochimica Acta Part A: Molecular and Biomolecular Spectroscopy](#) **53**, 2159 (1997).
- [9] P. Vandenabeele and M. Donais, *Mobile spectroscopic instrumentation in archaeometry research*, [Applied Spectroscopy](#) **70**, 27 (2016).
- [10] L. Struick van der Loeff, M. Alfeld, T. Meedendorp, J. Dik, E. Hendriks, G. Van der Snickt, K. Janssens, and M. Chavannes, *Van Gogh Studies* (Kröller-Müller Museum, 2012).
- [11] R. Hendrickx, G. Desmarais, M. Weder, E. S. Ferreira, and D. Derome, *Moisture uptake and permeability of canvas paintings and their components*, [Journal of Cultural Heritage](#) **19**, 445 (2016).
- [12] N. M. C. O. Poli T., Piccirillo A., *Interactions of natural resins and pigments in works of art*, [Journal of Colloid and Interface Science](#) **503**, 1 (2017).
- [13] S. Everts, *Art conservators struggle with microscopic eruptions in masterpieces*, [Chemical and Engineering News](#) **94**, 21 (2016).
- [14] J. L. Nasa, F. Modugno, M. Aloisi, A. Lluveras-Tenorio, and I. Bonaduce, *Development of a gc/ms method for the qualitative and quantitative analysis of mixtures of free fatty acids and metal soaps in paint samples*, [Analytica Chimica Acta](#) (2017), <https://doi.org/10.1016/j.aca.2017.11.017>.

- [15] A. Cesaratto, M. Leona, J. R. Lombardi, D. Comelli, A. Nevin, and P. Londero, *Detection of organic colorants in historical painting layers using uv laser ablation surface-enhanced raman microspectroscopy*, *Angewandte Chemie International Edition* **53**, 14373 (2014).
- [16] K. Janssens, M. Alfeld, G. Van der Snickt, W. De Nolf, F. Vanmeert, M. Radepont, L. Monico, J. Dik, M. Cotte, G. Falkenberg, C. Miliani, and B. Brunetti, *Annual review of analytical chemistry*, The Use of Synchrotron Radiation for the Characterization of Artists' Pigments and Paintings **6**, 399 (2013).
- [17] T. Trojek and D. Trojková, *Several approaches to the investigation of paintings with the use of portable x-ray fluorescence analysis*, *Radiation Physics and Chemistry* **116**, 321 (2015).
- [18] J.-W. Ha and S.-J. Lee, *Identification of natural inorganic pigments used on 18th century korean traditional mural paintings by using a portable x-ray fluorescence*, *Journal of Industrial and Engineering Chemistry* **28**, 328 (2015).
- [19] D. L. Howard, M. D. de Jonge, D. Lau, D. Hay, M. Varcoe-Cocks, C. G. Ryan, R. Kirkham, G. Moorhead, D. Paterson, and D. Thurrowgood, *High-definition x-ray fluorescence elemental mapping of paintings*, *Analytical Chemistry* **84**, 3278 (2012).
- [20] Z. Szökefalvi-Nagy, I. Demeter, A. Kocsonya, and I. Kovács, *Non-destructive xrf analysis of paintings*, *Nuclear Instruments and Methods in Physics Research Section B: Beam Interactions with Materials and Atoms* **226**, 53 (2004).
- [21] J. Dik, K. Janssens, G. Van Der Snickt, L. van der Loeff, K. Rickers, and M. Cotte, *Visualization of a lost painting by vincent van gogh using synchrotron radiation based x-ray fluorescence elemental mapping*, *Analytical Chemistry* **80**, 6436 (2008).
- [22] M. Gargano, F. Cavaliere, D. Viganò, A. Galli, and N. Ludwig, *A new spherical scanning system for infrared reflectography of paintings*, *Infrared Physics & Technology* **81**, 128 (2017).
- [23] N. Gao and I. Y. Ponomarev, *Polycapillary xray optics: manufacturing status, characterization and the future of the technology*, *XRay Spectrometry* **32**, 186 (2003).
- [24] A. R. Woll, D. H. Bilderback, S. Gruner, N. Gao, R. Huang, C. Bisulca, and J. Mass, *Development of confocal x-ray fluorescence (xrf) microscopy at the cornell high energy synchrotron source*, *Applied Physics* (2006).
- [25] A. R. Woll, N. Ocon, J. Mass, C. Bisulca, M. Cushman, C. Griggs, and T. Wazny, *The unique history of the armorers shop; an application of confocal x-ray fluorescence microscopy*, *Studies in Conservation* **53**, 93 (2008).
- [26] T. Trojek, R. Proke, R. efc, H. Bilavíková, and T. echák, *Confocal x-ray fluorescence spectrometer for in-situ analyses of paintings*, *Radiation Physics and Chemistry* **137**, 238 (2017).
- [27] K. Nakano, A. Tabe, S. Shimoyama, and K. Tsuji, *Visualizing a black cat drawing hidden inside the painting by confocal micro-xrf analysis*, *Microchemical Journal* **126**, 496 (2016).
- [28] M. Alfeld and J. A. Broekaert, *Mobile depth profiling and sub-surface imaging techniques for historical paintingsa review*, *Spectrochimica Acta Part B: Atomic Spectroscopy* **88**, 211 (2013).
- [29] I. Reiche, K. Muller, M. Eveno, E. Itie, and M. Menu, *Depth profiling reveals multiple paint layers of louvre renaissance paintings using non-invasive compact confocal micro-x-ray fluorescence*, *J. Anal. At. Spectrom.* **27**, 1715 (2012).

- [30] K. Wang, D.-W. Sun, and H. Pu, *Emerging non-destructive terahertz spectroscopic imaging technique: Principle and applications in the agri-food industry*, [Trends in Food Science & Technology](#) **67**, 93 (2017).
- [31] M. Koch, S. Hunsche, P. Schumacher, M. C. Nuss, J. Feldmann, and J. Fromm, *Thz-imaging: a new method for density mapping of wood*, [Wood Science and Technology](#) **32**, 421 (1998).
- [32] R. Groves, B. Pradarutti, E. Kouloumpi, W. Osten, and G. Notni, *2d and 3d non-destructive evaluation of a wooden panel painting using shearography and terahertz imaging*, [NDT & E International](#) **42**, 543 (2009).
- [33] M. Picollo, K. Fukunaga, and J. Labaune, *Obtaining noninvasive stratigraphic details of panel paintings using terahertz time domain spectroscopy imaging system*, [Journal of Cultural Heritage](#) **16**, 73 (2015).
- [34] K. Fukunaga and I. Hosako, *Innovative non-invasive analysis techniques for cultural heritage using terahertz technology*, [Comptes Rendus Physique](#) **11**, 519 (2010).
- [35] K. Fukunaga, I. Hosako, Y. Ogawa, and S. Hayashi, *Thz spectroscopy for art conservation science, 2007 Joint 32nd International Conference on Infrared and Millimeter Waves and the 15th International Conference on Terahertz Electronics*, 678 (2007).
- [36] J. B. Jackson, J. Bowen, G. Walker, J. Labaune, G. Mourou, M. Menu, and K. Fukunaga, *A survey of terahertz applications in cultural heritage conservation science*, [IEEE Transactions on Terahertz Science and Technology](#) **1**, 220 (2011).
- [37] H. Zhang, S. Sfarra, K. Saluja, J. Peeters, J. Fleuret, Y. Duan, H. Fernandes, N. Avdelidis, C. Ibarra-Castanedo, and X. Maldague, *Non-destructive investigation of paintings on canvas by continuous wave terahertz imaging and flash thermography*, [Journal of Nondestructive Evaluation](#) **36**, 34 (2017).
- [38] F. Kim, S. Moylan, E. Garboczi, and J. Slotwinski, *Investigation of pore structure in cobalt chrome additively manufactured parts using x-ray computed tomography and three-dimensional image analysis*, [Additive Manufacturing](#) **17**, 23 (2017).
- [39] K. Krug, L. Porra, P. Coan, A. Wallert, J. Dik, A. Coerdts, A. Bravin, M. Elyyan, P. Reischig, Helfen, and T. L. Baumbach, *Relics in medieval altarpieces? combining x-ray tomographic, lamino-graphic and phase-contrast imaging to visualize thin organic objects in paintings*, [Journal of Synchrotron Radiation](#) **15**, 55 (2008).
- [40] J. T. D. III and D. J. Godfrey, *Digital x-ray tomosynthesis: current state of the art and clinical potential*, [Physics in Medicine & Biology](#) **48**, R65 (2003).
- [41] T. Villafanna, W. Brown, J. Delaney, M. Palmer, W. W.S., and F. M.C., *Femtosecond pump-probe microscopy generates virtual cross-sections in historic artwork*, [P NATLACAD SCI USA](#) **111**, 1708 (2014).
- [42] F. Alam, S. U. Rahman, S. Ullah, and K. Gulati, *Medical image registration in image guided surgery: Issues, challenges and research opportunities*, [Biocybernetics and Biomedical Engineering](#) **38**, 71 (2018).
- [43] A. Cosentino, *Fors spectral database of historical pigments in different binders*, [E-conservation Journal](#) **2**, 57 (2014).

-
- [44] P. Hansen, V. Pereyra, and G. Scherer, *Least Squares Data Fitting with Applications*, Least Squares Data Fitting with Applications (Johns Hopkins University Press, 2012) pp. 171–173.
- [45] L. Hoogstede, R. Spronk, R. Erdmann, and R. Gotink, *Hieronymus Bosch: Painter and Draughtsman. Technical Studies* (Mercatorfonds, 2016) pp. 49–51.